1
Entropy and Renormalization in Chaotic Visibility Graphs

Bartolo Luque, Fernando Jesús Ballesteros, Alberto Robledo, and Lucas Lacasa

In this chapter, we concentrate on a mapping from time series to graphs, the visibility algorithm introduced by Lacasa *et al.* [1]. In order to cite some of its most relevant features, we will stress its intrinsic nonlocality, low computational cost, straightforward implementation, and quite "simple" way of inheriting the time series properties in the structure of the associated graphs. These features will make it easier to find connections between the underlying processes and the networks obtained from them by a direct analysis of the latter. In particular, in this chapter, we will focus the implementation of the algorithm of visibility to three known routes to chaos. We will define a graph entropy and process of renormalization for visibility graphs that characterize these routes and analyze the relationship between the flow of renormalization and the extremes of the entropy function.

Disregarding any underlying process, we can consider a time series just as an ordered set of values and transform this set into a different mathematical object with the aids of an abstract mapping [2, 3]. We can then ask which properties of the original set are conserved, which are transformed and how, what can we say about one of the mathematical representations just by looking at the other. This exercise is of mathematical interest by itself. In addition, it turns out that time series or signals is a universal method of extracting information from dynamical systems in any field of science. Therefore, the preceding mathematical mapping gains some unexpected practical interest as it opens the possibility of analyzing a time series from an alternative point of view. Of course, the relevant information stored in the original time series should be somehow conserved in the mapping. The motivation is completed when the new representation belongs to a relatively mature mathematical field, where information encoded in such a representation can be effectively disentangled and processed. This is, precisely, the first motivation to map time series into networks.

This motivation is increased by two interconnected factors: (i) Although a mature field, time series analysis has some limitations, when it refers to study the so-called complex signals. Beyond the linear regime, there exists a wide range of phenomena, which are usually embraced in the field of the so-called

Mathematical Foundations and Applications of Graph Entropy, First Edition.
Edited by Matthias Dehmer, Frank Emmert-Streib, Zengqiang Chen, Xueliang Li, and Yongtang Shi.

complex systems. Dynamical phenomena such as chaos, long-range correlated stochastic processes, intermittency, and multifractality are examples of complex phenomena, where time series analysis is pushed to its own limits. Nonlinear time series analysis develops from techniques such as nonlinear correlation functions, embedding algorithms, multrifractal spectra, and projection theorem tools that increase in complexity parallel to the complexity of the process/series under study. New approaches to deal with complexity are not only welcome, but needed. Approaches dealing with the intrinsic nonlinearity by being intrinsically nonlinear in turn deal with the possible multiscale character of the underlying process by being designed to naturally incorporated multiple scales, and such is the framework of networks, of graph theory. (ii) The technological era brings us the possibility to digitally analyze myriads of data in a glimpse. Massive data sets can nowadays be parsed, and with the aid of well-suited algorithms, we can gain access and filter data from many processes, let it be of physical, technological, or even social garment.

1.1 Mapping Time Series to Networks

The idea of mapping time series into graphs seems attractive, because it bridges two prolific fields of modern science as nonlinear signal analysis and complex networks theory, as much that it has attracted the attention of several research groups, which have contributed to the topic with different strategies of mapping. We shall briefly outline some of them.

Zhang and Small [4] developed a method that mapped each cycle of a pseudo-periodic time series into a node in a graph. The connection between nodes was established by a distance threshold in the reconstructed phase space when possible or by the linear correlation coefficient between cycles in the presence of noise. Noisy periodic time series mapped into random graphs while chaotic time series did it into scale-free, small-world networks due to the presence of unstable periodic orbits. This method was subsequently applied to characterize cardiac dynamics.

Xu, in collaboration with Zhang and Small [5], concentrated in the relative frequencies of appearance of four-node motifs inside a particular graph to classify it into a particular superfamily of networks, which corresponded to specific underlying dynamics of the mapped time series. In this case, the method of mapping consisted in embedding the time series in an appropriated phase space, where each point corresponded to a node in the network. A threshold was imposed not only in the minimum distance between two neighbors to be eligible (temporal separation should be greater than the mean period of the data), but also to the maximum number of neighbors a node could have. Different superfamilies were found for chaotic, hyperchaotic, random, and noisy periodic underlying dynamics and unique fingerprints were also found for specific dynamical systems within a family.

Donner *et al.* [6–8] presented a technique, which was based on the properties of recurrence in the phase space of a dynamical system. More precisely, the recurrence matrix obtained by imposing a threshold in the minimum distance between two points in the phase space was interpreted as the adjacency matrix of an undirected, unweighted graph (as in Ref. [5]). Properties of such graphs at three different scales (local, intermediated, and global) were presented and studied on several paradigmatic systems (Hénon map, Rossler system, Lorenz system, and Bernoulli map). The variation of some of the properties of the graphs with the distance threshold was analyzed, the use of specific measures, such as the local clustering coefficient, was proposed as a way to detect dynamically invariant objects (saddle points or unstable periodic orbits), and studying the graph properties dependent on the embedding dimension was suggested as a means to distinguish between chaotic and stochastic systems.

The Amaral Lab [9] contributed with an idea along the lines of Shirazi *et al.* [10], Strozzi *et al.* [11], and Haraguchi *et al.* [12] of a surjective mapping, which admits an inverse operation. This approach opens the reciprocal possibility of benefiting from time series analysis to study the structure and properties of networks. Time series are treated as Markov processes, and values are grouped in quantiles, which will correspond to nodes in the associated graph. Weighted and directed connections are established between nodes as a function of the probability of transition between quantiles. An inverse operation can be defined without an a priori knowledge of the correspondence between nodes and quantiles just by imposing a continuity condition in the time series by means of a cost function defined on the weighted adjacency matrix of the graph. A random walk is performed on the network and a time series with properties equivalent to the original one is recovered. This method was applied to a battery of cases, which included a periodic-to-random family of processes parameterized by a probability of transition, a pair of chaotic systems (Lorentz and Rossler attractors), and two human heart rate time series. Reciprocally, the inverse map was applied to the metabolic network of Arabidopsis thaliana and to the '97 year Internet Network.

In the same vein of an inverse transformation, Shimada *et al.* [13] proposed a framework to transform a complex network to a time series, realized by a multidimensional scaling. Applying the transformation method to a model proposed by Watts and Strogatz [14], they show that ring lattices are transformed to periodic time series, small-world networks to noisy periodic time series, and random networks to random time series. They also show that these relationships are analytically held by using the circulant matrix theory and the perturbation theory of linear operators. They generalize the results to several high-dimensional lattices.

Gao and Jin proposed in Ref. [15] a method for constructing complex networks from a time series with each vector point of the reconstructed phase space represented by a single node and edge determined by the phase space distance. Through investigating an extensive range of network topology statistics, they find that the constructed network inherits the main properties of the time series in its structure. Specifically, periodic series and noisy series convert into regular networks and random networks, respectively, and networks generated from chaotic series

typically exhibit small-world and scale-free features. Furthermore, they associate different aspects of the dynamics of the time series with the topological indices of the network and demonstrate how such statistics can be used to distinguish different dynamical regimes. Through analyzing the chaotic time series corrupted by measurement noise, they also indicate the antinoise ability of the method.

Sinatra *et al.* [16] introduced a method to convert an ensemble of sequences of symbols into a weighted directed network, whose nodes are motifs, while the directed links and their weights are defined from statistically significant co-occurrences of two motifs in the same sequence. The analysis of communities of networks of motifs is shown to be able to correlate sequences with functions in the human proteome database, to detect hot topics from online social dialogs and characterize trajectories of dynamical systems.

Sun *et al.* [17] have also proposed a novel method to transform a time series into a weighted and directed network. For a given time series, they first generate a set of segments via a sliding window, and then use a doubly symbolic scheme to characterize every windowed segment by combining absolute amplitude information with an ordinal pattern characterization. On the basis of this construction, a network can be directly constructed from the given time series: segments corresponding to different symbol-pairs are mapped to network nodes and the temporal succession between nodes is represented by directed links. With this conversion, dynamics underlying the time series has been encoded into the network structure. They illustrate the potential of their networks with a well-studied dynamical model as a benchmark example. Results show that network measures for characterizing global properties can detect the dynamical transitions in the underlying system. Moreover, they used a random walk algorithm to sample loops in networks, and found that a time series with different dynamics exhibits distinct cycle structure. That is, the relative prevalence of loops with different lengths can be used to identify the underlying dynamics.

In the following, we will first present two versions of the visibility algorithm, our own alternative to these methods of mapping, along with its most notable properties that, in many cases, can be derived analytically. On the basis of these latter properties, several applications are addressed.

1.1.1
Natural and Horizontal Visibility Algorithms

Let $\{x(t_i)\}_{i=1,\ldots,N}$ be a time series of N data. The natural visibility algorithm [1] assigns each datum of the series to a node in the natural visibility graph (NVg). Two nodes i and j in the graph are connected if one can draw a straight line in the time series joining $x(t_i)$ and $x(t_j)$ that does not intersect any intermediate data height $x(t_k)$ (see Figure 1.1 for a graphical illustration). Hence, i and j are two connected nodes if the following geometrical criterion is fulfilled within the time series:

$$x(t_k) < x(t_i) + (x(t_j) - x(t_i))\frac{t_k - t_i}{t_j - t_k}. \tag{1.1}$$

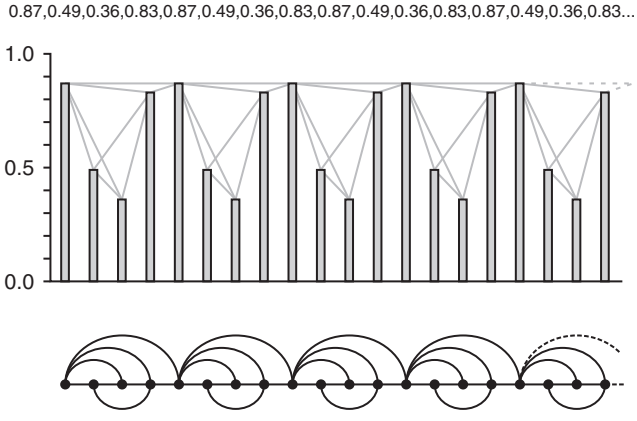

Figure 1.1 Illustrative example of the natural visibility algorithm. In the upper part, we plot a periodic time series and in the bottom part, we represent the graph generated through the natural visibility algorithm. Each datum in the series corresponds to a node in the graph, such that two nodes are connected if their corresponding data heights fulfill the visibility criterion of equation 1.1. Note that the degree distribution of the visibility graph is composed by a finite number of peaks, much in the vein of the discrete Fourier transform (DFT) of a periodic signal. We can thus interpret the visibility algorithm as a geometric transform. (Luque *et al.* [18]. Reproduced with permission of American Physical Society.)

It can be easily checked that by means of the present algorithm, the associated graph extracted from a time series is always:

(i) Connected: each node sees at least its nearest neighbors (left- and right-hand sides).
(ii) Undirected: the way the algorithm is built up, there is no direction defined in the links.
(iii) Invariant under affine transformations of the series data: the visibility criterion is invariant under (unsigned) linear rescaling of both horizontal and vertical axis, as well as under horizontal and vertical translations.
(iv) "Lossy": some information regarding the time series is inevitably lost in the mapping from the fact that the network structure is completely determined in the adjacency matrix. For instance, two periodic series with the same period as $T_1 = \ldots, 3, 1, 3, 1, \ldots$ and $T_2 = \ldots, 3, 2, 3, 2, \ldots$ would have the same visibility graph, albeit being quantitatively different.

One straightforward question is: what does the visibility algorithm stand for? In order to deepen the geometric interpretation of the visibility graph, let us focus on a periodic series. It is straightforward that its visibility graph is a concatenation of a motif: a repetition of a pattern (see Figure 1.1). Now, which is the degree distribution $p(k)$ of this visibility graph? Since the graph is just a motif's repetition, the degree distribution will be formed by a finite number of nonnull values, this number being related to the period of the associated periodic series.

This behavior reminds us the DFT, in which periodic series is formed by a finite number of peaks (vibration modes) related to the series period. Using this analogy, we can understand the visibility algorithm as a geometric transform. Whereas a DFT decomposes a signal in a sum of (eventually infinite) modes, the visibility algorithm decomposes a signal in a concatenation of graph's motifs, and the degree distribution simply makes a histogram of such "geometric modes." While the time series is defined in the time domain and the DFT is defined on the frequency domain, the visibility graph is then defined on the "visibility domain." In fact this analogy is, so far, a simple metaphor to help our intuition, this transform is not a reversible one for instance.

An alternative criterion for the construction of the visibility graph is defined as follows: let $\{x(t_i)\}_{i=1,\ldots,N}$ be a time series of N data. The so-called horizontal visibility algorithm [18] assigns each datum of the series to a node in the horizontal visibility graph (HVg). Two nodes i and j in the graph are connected if one can draw a horizontal line in the time series joining $x(t_i)$ and $x(t_j)$ that does not intersect any intermediate data height (see Figure 1.2 for a graphical illustration). Hence, i and j are two connected nodes if the following geometrical criterion is fulfilled within the time series:

$$x(t_i), x(t_j) > x(t_n) \quad \text{for all } n \text{ such that } i < n < j. \tag{1.2}$$

This algorithm is a simplification of the Natural Visibility algorithm (NVa). In fact, the HVg is always a subgraph of its associated NVg for the same time series (see Figure 1.2). Besides, the HVg graph will also be (i) connected, (ii) undirected, (iii) invariant under affine transformations of the series, and (iv) "lossy." Some concrete properties of these graphs can be found in Refs [18–21]. HVg method is quite more tractable analytically than NVg. Hence, for example, if $\{x_i\}$ is a bi-infinite sequence of independent and identically distributed random variables extracted from a continuous probability density $f(x)$, then its associated HVg has degree distribution:

$$p(k) = \frac{1}{3}\left(\frac{2}{3}\right)^{k-2}, \quad k = 2, 3, 4, \ldots . \tag{1.3}$$

A lengthy constructive proof can be found in Ref. [18] and alternative, shorter proofs can be found in Ref. [22]. The mean degree $\overline{k}$ of the HVg associated to an uncorrelated random process is then:

$$\overline{k} = \sum kp(k) = \sum_{k=2}^{\infty} \frac{k}{3}\left(\frac{2}{3}\right)^{k-2} = 4. \tag{1.4}$$

In fact, the mean degree of an HVg associated to an infinite periodic series of period T (with no repeated values within a period) is

$$\overline{k}(T) = 4\left(1 - \frac{1}{2T}\right). \tag{1.5}$$

A proof can be found in Ref. [22]. An interesting consequence is that every time series has an associated HVg with a mean degree $2 \leq \overline{k} \leq 4$, where the lower bound is reached for constant series, whereas the upper bound is reached for aperiodic series [18].

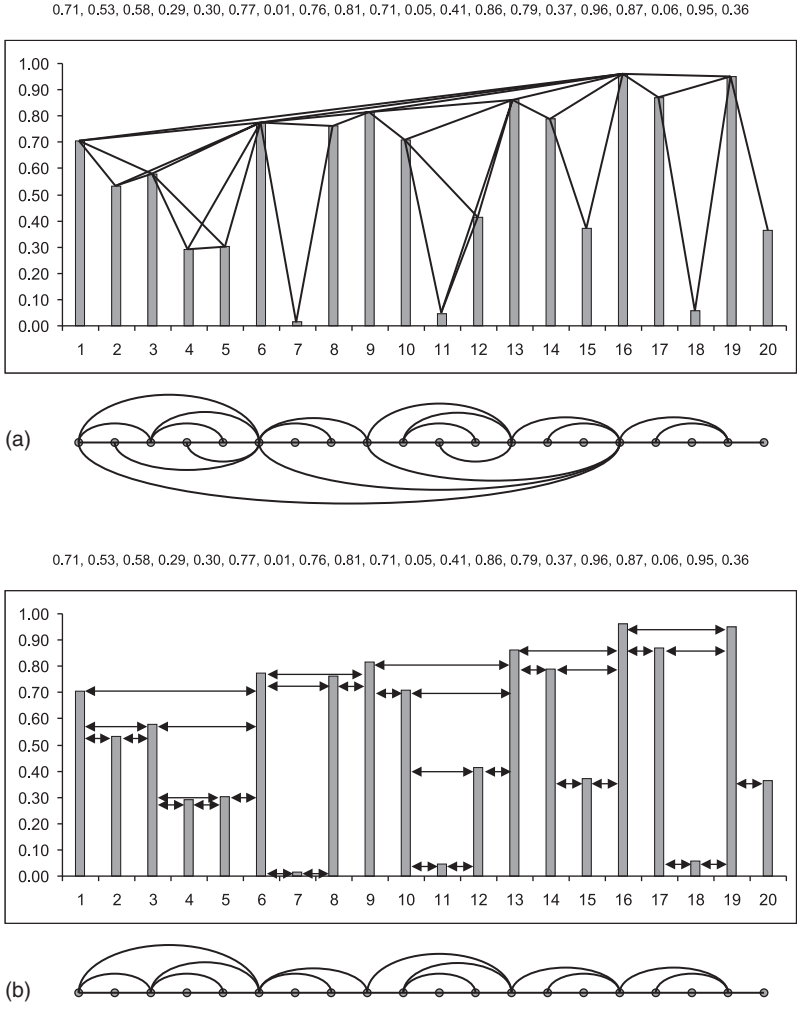

Figure 1.2 Illustrative example of the Natural (a) and Horizontal (b) visibility algorithms. We plot the same time series and represent the graphs generated through both visibility algorithms below. Each datum in the series corresponds to a node in the graph, such that two nodes are connected if their corresponding data heights fulfill the visibility criteria of equations 1.1 and 1.2, respectively. Observe that the Horizontal Visibility graph is a subgraph of the Natural Visibility graph for the same time series. (Luque *et al.* [18]. Reproduced with permission of American Physical Society.)

1.1.2 A Brief Overview of Some Initial Applications

In order to end this introduction without intending to be exhaustive, we believe appropriate to point out some of the areas where, despite the recent method, the visibility algorithm has been applied with interesting results:

1.1.2.1 Seismicity

Aguilar-San Juan and Guzman-Vargas presented, in Ref. [23], a statistical analysis of earthquake magnitude sequences in terms of the visibility graph method. Magnitude time series from Italy, southern California, and Mexico are transformed into networks and some organizational graph properties are discussed. Connectivities are characterized by a scale-free distribution with a notable effect for large scales due to either the presence or absence of large events. In addition, a scaling behavior is observed between different node measures such as betweenness centrality, clustering coefficient, nearest-neighbor connectivity, and earthquake magnitude. Moreover, parameters which quantify the difference between forward and backward links are proposed to evaluate the asymmetry of visibility attachment mechanism. Their results show an alternating average behavior of these parameters as earthquake magnitude changes. Finally, they evaluate the effects of reducing temporal and spatial windows of observation upon visibility network properties for main shocks.

Telesca *et al.* [24–26] have analyzed the synthetic seismicity generated by a simple stick-slip system with asperities by using the method of the visibility graph. The stick-slip system mimics the interaction between tectonic plates, whose asperities are given by sandpapers of different granularity degrees. The visibility graph properties of the seismic sequences have been put in relationship with the typical seismological parameter, the b-value of the Gutenberg–Richter law. Between the b-value of the synthetic seismicity and the slope of the least-square line fitting, the $k-M$ plot (relationship between the magnitude M of each synthetic event and its connectivity degree k), a close linear relationship is found, which is verified by real seismicity.

1.1.2.2 Hurricanes

Elsner *et al.* [27] demonstrated the method of construction of a network from a time series of US hurricane counts and showed how it can be used to identify unusual years in the record. The network links years based on a line-of-sight visibility algorithm applied to the time series plot and is physically related to the variation of hurricanes from 1 year to the next. The authors find that the distribution of node degree is consistent with a random Poisson process. High hurricane-occurrence years that are surrounded by years with few hurricanes have many linkages. Of the environmental conditions known to affect coastal hurricane activity, they find years with little sunspot activity during September (peak month of the hurricane season) best correspond with the unusually high linkage years.

1.1.2.3 Turbulence

A classic topic in fluid mechanics is the complex behavior exhibited by some fluids within a certain regime, characterized basically by a dimensionless number known as Reynolds number, consisting of a high-dimensional spatiotemporal form of chaos called turbulence. The multiscale nature of this phenomenon is reflected in the distribution of velocity increments and energy dissipation rates, which exhibit anomalous scalings suggesting some kind of multifractality. A first attempt to characterize an energy dissipation rate time series by means of the visibility algorithm was made by Liu *et al.* [28]. In this work, a series obtained from wind tunnel experimental measurements was mapped into a graph by the natural visibility version of the algorithm yielding a power law of exponent $\gamma = 3.0$ for the degree distribution. An edge covering box-counting method was used to prove the nonfractality of the graph and allometric scalings for the skeleton and random spanning trees of the graph were proposed, but no functional relation to any physical magnitude characterizing the phenomenon could be derived.

1.1.2.4 Financial Applications

Yang *et al.* [29] mapped six exchange rate series and their corresponding detrended series into graphs by means of the NVa. The results suggest that, for certain purposes, these series can be modeled as fractional Brownian motions. The multifractal structure of the series was broken by shuffling them and so, shuffled series mapped into graphs with exponential degree distributions.

Qian *et al.* [30], in the same philosophy as Liu *et al.* [28], built three different classes of spanning trees from the graphs associated to 30 world stock market indices and studied their allometric properties, finding universal allometric scaling behavior in one of the classes. No satisfactory explanation was found for this fact. They also built spanning trees from graphs associated to fractional Brownian motions with different Hurst exponents, finding discrepancies in their allometric behavior with the ones mapped from the stock market indices. These discrepancies were attributed to the nonlinear long-term correlations and fat-tailed distributions of the financial series.

1.1.2.5 Physiology

Shao [31] used the visibility algorithm to construct the associated networks of time series of filtered data of five healthy subjects and five patients with congestive heart failure (CHF). He used the assortative coefficient of the networks to distinguish healthy patients from CHF patients. On the contrary, Dong and Liâ [32], in a comment on the first work, calculated the assortativity coefficients of heartbeat networks extracted from time series of healthy subjects and CHF patients and concluded that the assortative coefficients of such networks failed as an effective indicator to differentiate healthy patients from CHF patients at large.

Ahmadlou *et al.* [33] presented a new chaos-wavelet approach for electroencephalogram (EEG)-based diagnosis of Alzheimer's disease (AD) using the visibility graph. The approach is based on the research ideology that nonlinear features may not reveal differences between AD and control group in the

band-limited EEG, but may represent noticeable differences in certain subbands. Hence, complexity of EEGs is computed using the VGs of EEGs and EEG subbands produced by wavelet decomposition. Two methods are used for computation of complexity of the VGs: one based on the power of scale-freeness of a graph structure and the other based on the maximum eigenvalue of the adjacency matrix of a graph. Analysis of variation is used for feature selection. Two classifiers are applied to the selected features to distinguish AD and control EEGs: a radial basis function neural network (RBFNN) and a two-stage classifier consisting of principal component analysis (PCA) and RBFNN. After comprehensive statistical studies, effective classification features and mathematical markers are presented.

1.2 Visibility Graphs and Entropy

1.2.1 Definitions of Entropy in Visibility Graphs

Following the pioneering works of Rashevsky [34] and Trucco [35], the use of entropy in graphs was introduced by A. Mowshowitz in 1968 [36] to characterize the complexity of a graph. Soon afterward, Korner in 1971 [37] applied a different definition of the concept to solve a coding problem formulated in information theory. Since then, various graph entropy measures have been developed, reinvented, and applied to a diversity of situations (see [38] for a review). Shannon [39] defined the entropy of any set of probabilities $\{p_i\}$ as $H = -\sum p_i \log p_i \geq 0$, where p_i is the probability of occurrence of the event i, but what is the meaning of p_i in a graph? Here we can consider several possibilities. For example, p_i could be the probability that a vertex in the graph has a degree $k = i$, hence we can rename it as $p(k)$, and thus the graph entropy becomes:

$$h = -\sum_k p(k) \log p(k). \tag{1.6}$$

Another possibility could be to consider clustering rather than degree, using $p(C)$ instead. However, clustering is computationally harder to obtain, and it is very easy to prove that $-\sum p(C) \log p(C)$ produces exactly the same value as Eq. 1.6. Other alternatives (as the probability of having two nodes connected, etc.) do not produce significantly different results; thus, for the following, we will use the degree distribution and define as *graph entropy* the one defined by Eq. 1.6 (note that in directed graphs, one could also consider the *in* and *out* degree distributions and hence define h_{in} and h_{out}).

In the case of visibility graphs coming from time series, the graph entropy h is strongly linked to the Shannon entropy H of its corresponding time series $x(t)$, given by $H = -\sum p(x) \log p(x)$ as at the end of the day, the information in the visibility graph comes from the time series. Therefore, the graph entropy of the

visibility graph is a very good proxy of the Shannon entropy for the associated time series.

Graph entropy is obtained from the whole structure of the graph, and hence is a static magnitude. However, as visibility graphs come from dynamic processes, one should consider the role of entropies linked to such processes. Thus, in an iterative process, one can consider the Kolmogorov–Sinai entropy [40, 41], which was introduced to solve the "isomorphism problem," that is, whether there is a mapping between two seemingly different dynamical systems, preserving the dynamical and statistical relationships between the successive states. As H_{KS} is invariant under any isomorphism, two dynamical systems with different values for H_{KS} are nonisomorphic. H_{KS} can be defined as the rate of increment of entropy along the transformation T: Let us consider an abstract space Ω with a probability measure μ that assigns probabilities to subsets of Ω. Let us make a partition A of Ω composed by separate subsets $A_1, A_2, \ldots, A_n$ such that their union is Ω. The probability assigned to each subset is $p_i = \mu(A_i)$, $\mathrm{P}_A = (p_1, p_2, \ldots, p_n)$ and its Shannon entropy is $h(\mathrm{P}_A) = -\sum p_i \log p_i$. Let us consider T a dynamic transformation in Ω, leaving invariant the probabilities: $p_i = \mu(A_i) = \mu(T^{-1}(A_i))$. After m iterations of this transformation, we define A^m as $A \vee T^{-1}(A) \vee T^{-2}(A) \ldots \vee T^{-m+1}(A)$. For this given partition A and iterative process T, the Kolmogorov–Sinai entropy is given by

$$H_{\mathrm{KS}}(T, A) = \lim_{m \to \infty} \frac{1}{m} H(\mathrm{P}_{A^m}). \tag{1.7}$$

It represents the increase of entropy due to the transformation T in the partition A. Note that, for $m = 1$, that is, for a single-step process, Kolmogorov–Sinai entropy is equal to Shannon entropy.

In order to consider the entropy rate due purely to T, regardless of the partition considered, one has to take into account all the infinite possible partitions and keep the partition, which produces the higher value:

$$H_{\mathrm{KS}}(T) = \sup_A H_{\mathrm{KS}}(T, A). \tag{1.8}$$

In the case of chaotic time series, Kolmogorov–Sinai entropy exhibits a very interesting property, thanks to the Pesin theorem [42]. This theorem states an intimate relationship between H_{KS} and the positive Lyapunov exponents given by

$$H_{\mathrm{KS}} \leq \sum_{i, \gamma_i \geq 0} \gamma_i = \sum_i \gamma_i^+. \tag{1.9}$$

This inequality, known as Pesin inequality, turns into an equality for sufficiently chaotic systems. Thus, for a deterministic dynamics, Kolmogorov–Sinai entropy is a criterion and quantitative index of chaos [43, 44]. The relevance of Kolmogorov–Sinai entropy in data analysis to globally quantify the temporal organization of the evolution has been recognized in numerous applications, and it is now a standard tool of nonlinear time series analysis.

Block entropy is another way to link Kolmogorov–Sinai entropy and Shannon entropy. For a stationary stochastic process $(x_t)_{t \geq 0}$ (in discrete time t), Shannon

entropy of the array $(x_1,\ldots,x_n)$ is termed block entropy of order n and denoted H_n. It is the Shannon entropy of the n-word distribution, namely:

$$H_n = -\frac{1}{n}\sum_{x_1\ldots x_n} p(x_1 \ldots x_n)\log p(x_1 \ldots x_n). \tag{1.10}$$

The n-block entropy captures quantitatively correlations of range shorter than n, by contrast with the simple entropy $H = H_1$, which is only sensitive to the frequencies of the different elementary states. The Kolmogorov–Sinai entropy can be recovered from the block entropy [45] as the asymptotic limit of block entropies. Taking advantage of this fact, we can define for a visibility graph an analogous set of *graph* block entropies related to the degrees of the graph, as

$$h_n = -\frac{1}{n}\sum_{k_1\ldots k_n} p(k_1 \ldots k_n)\log p(k_1 \ldots k_n). \tag{1.11}$$

And its asymptotic limit will be an analogue to the Kolmogorov–Sinai entropy, but for the visibility graph, that is, the *graph* Kolmogorov–Sinai entropy:

$$h_{\mathrm{KS}} = \lim_{n\to\infty} h_n. \tag{1.12}$$

1.2.2
Pesin Theorem in Visibility Graphs

The period-doubling bifurcation cascade or Feigenbaum scenario is perhaps the better known and most famous route to chaos [46, 47]. This route to chaos appears an infinite number of times among the family of attractors spawned by unimodal maps within the so-called periodic windows that interrupt stretches of chaotic attractors. Their shared bifurcation accumulation points form transitions between order and chaos that are known to exhibit universal properties [48].

A general observation is that the HVg extracts not only universal elements of the dynamics, free of the peculiarities of the individual unimodal map, but also of universality classes characterized by the degree of nonlinearity. Therefore, all the results presented in the following, while referring to the specific logistic map for illustrative reasons, apply to any unimodal map. In the case of the Feigenbaum scenario, these graphs are named *Feigenbaum graphs*.

Logistic map is defined by the quadratic difference equation $x_{t+1} = f(x_t) = \mu x_t(1 - x_t)$, where $x_t \in [0, 1]$ and the control parameter $\mu \in [0, 4]$. According to the horizontal visibility (HV) algorithm, a time series generated by the logistic map for a specific value of μ (after an initial transient of approach to the attractor) is converted into a Feigenbaum graph (see Figure 1.3). This is a well-defined subclass of HV graphs, where consecutive nodes of degree $k = 2$, that is, consecutive data with the same value, do not appear, what is actually the case for series extracted from maps (besides the trivial case of a constant series).

A deep-seated feature of the period-doubling cascade is that the order in which the positions of a periodic attractor are visited is universal [50], the same for all

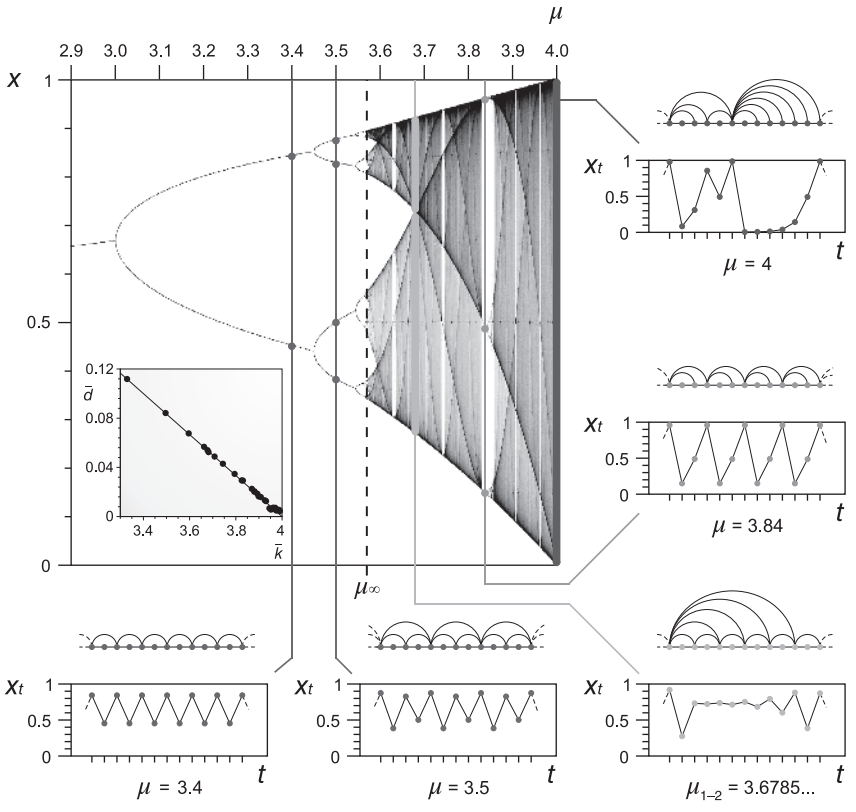

Figure 1.3 Feigenbaum graphs from the logistic map $x_{t+1} = f(x_t) = \mu x_t(1 - x_t)$. The main figure portrays the family of attractors of the logistic map and indicates a transition from periodic to chaotic behavior at $\mu_\infty = 3.569946\ldots$ through period-doubling bifurcations. For $\mu \geq \mu_\infty$, the figure shows merging of chaotic-band attractors, where aperiodic behavior appears interrupted by windows that, when entered from their left-hand side, display periodic motion of period $T = m \cdot 2^0$ with $m > 1$ (for $\mu < \mu_\infty$, $m = 1$) that subsequently develops into m period-doubling cascades with new accumulation points $\mu_\infty(m)$. (Luque *et al.* [49]. Reproduced with permission of American Institute of Physics.)

unimodal maps. This ordering turns out to be a decisive property in the derivation of the structure of the Feigenbaum graphs. See Figure 1.4, which plots the graphs for a family of attractors of increasing period $T = 2^n$, that is, for increasing values of $\mu < \mu_\infty$. This basic pattern also leads to the expression for their associated degree distributions at the n-th period-doubling bifurcation:

$$p(n,k) = \left(\tfrac{1}{2}\right)^{k/2}, \quad k = 2, 4, 6, \ldots, 2n,$$
$$p(n,k) = \left(\tfrac{1}{2}\right)^{n}, \quad k = 2(n+1), \tag{1.13}$$

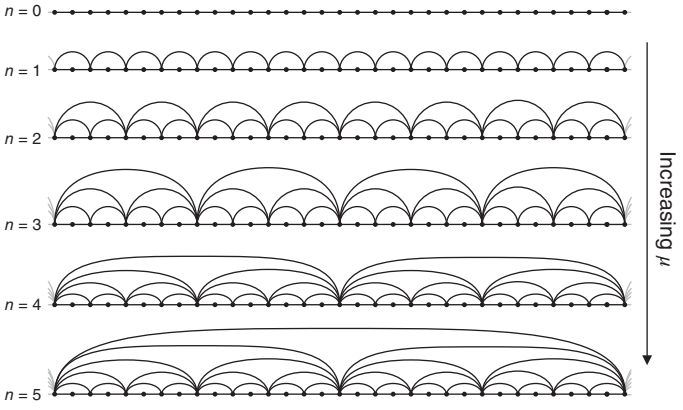

Figure 1.4 Periodic Feigenbaum graphs for $\mu < \mu_\infty$. The sequence of graphs associated to periodic attractors with increasing period $T = 2^n$ undergoing a period-doubling cascade. The pattern that occurs for increasing values of the period is related to the universal ordering with which an orbit visits the points of the attractor. Observe that the hierarchical self-similarity of these graphs requires that the graph for $n-1$ is a subgraph of that for n. (Luque *et al.* [49]. Reproduced with permission of American Institute of Physics.)

and zero for k odd or $k > 2(n+1)$. At the accumulation point μ_∞, the period diverges ($n \to \infty$) and the distribution is exponential for all even values of the degree,

$$p(\infty, k) = \left(\frac{1}{2}\right)^{k/2}, \quad k = 2, 4, 6, \ldots, \tag{1.14}$$

and zero for k odd.

By making use of the expression we have for the degree distribution $p(n,k)$ in the region $\mu < \mu_\infty$, we obtain for the graph entropy $h(n)$ after the nth period-doubling bifurcation (do not confuse with block entropy h_n), the following result:

$$\begin{aligned} h(n) &= -\sum_{k=2}^{2(n+1)} p(n,k) \log p(n,k) \\ &= -\sum_{k=2}^{2n} \frac{1}{2^{k/2}} \log\left(\frac{1}{2^{k/2}}\right) - \frac{1}{2^n} \log\left(\frac{1}{2^n}\right) \\ &= \frac{\log 2}{2}\left(\overline{k} - \frac{2}{2^n}\right) = \log 4 \left(1 - \frac{1}{2^n}\right). \end{aligned} \tag{1.15}$$

We observe that the graph entropy increases with n and, interestingly, depends linearly on the mean degree $\overline{k}$. This linear dependence between h and $\overline{k}$ is related to the fact that, generally, the entropy and the mean of a probability distribution are proportional to exponentially distributed functions, a property that holds exactly in the accumulation point (eq. 1.14) and approximately in the periodic region (eq. 1.13), where there is a finite cutoff that ends the exponential law. Finally, note

that in the limit $n \to \infty$ (accumulation point), the entropy converges to a finite value $h(\infty) = \log 4$.

Something similar happens in the chaotic region of the logistic map. Here, we find a period-doubling bifurcation cascade of chaotic bands that takes place as μ decreases from $\mu = 4$ to μ_∞. For the largest value of the control parameter, at $\mu = 4$, the attractor is fully chaotic and occupies the entire interval $[0, 1]$ (see Figure 1.3). This is the first chaotic band $n = 0$ at its maximum amplitude. As μ decreases in value within $\mu_\infty < \mu < 4$ band-narrowing and successive band-splittings [46–48, 50] occur. In general, after n reverse bifurcations, the phase space is partitioned in 2^n disconnected chaotic bands, which are self-affine copies of the first chaotic band [51]. The values of μ at which the bands split are called Misiurewicz points [50], and their location converges to the accumulation point μ_∞ for $n \to \infty$. Significantly, while in the chaotic zone orbits are aperiodic, for reasons of continuity, they visit each of the 2^n chaotic bands in the same order as positions are visited in the attractors of period $T = 2^n$ [50]. In Figure 1.5, we have plotted the Feigenbaum graphs generated through chaotic time series at different values of μ that correspond to an increasing number of reverse bifurcations. Since chaotic bands do not overlap, one can derive the following degree distribution for a Feigenbaum graph in the chaotic zone after n chaotic-band reverse bifurcations by using only the universal order of visits

$$p_\mu(n,k) = \left(\tfrac{1}{2}\right)^{k/2}, \quad k = 2, 4, 6, \ldots, 2n,$$
$$p_\mu(n, k \geq 2(n+1)) = \left(\tfrac{1}{2}\right)^{n}, \tag{1.16}$$

and zero for $k = 3, 5, 7, \ldots, 2n + 1$. We note that this time, the degree distribution retains some dependence on the specific value of μ, concretely, for those nodes with degree $k \geq 2(n + 1)$, all of which belong to the top chaotic band (labeled with dashed links in Figure 1.5). The HV algorithm filters out chaotic motion within all bands except for that taking place in the top band, whose contribution decreases as $n \to \infty$ and appears coarse-grained in the cumulative distribution $p_\mu(n, k \geq 2(n + 1))$. As would be expected, at the accumulation point μ_∞, we recover the exponential degree distribution (Eq. 1.14), i.e., $\lim_{n\to\infty} p_\mu(n, k) = p(\infty, k)$.

Regarding graph entropy in the chaotic zone, in general h cannot be derived exactly since the precise shape of $p_\mu(k)$ is unknown (albeit the asymptotic shape is also exponential). However, arguments of self-affinity similar to those used for describing the degree distribution of Feigenbaum graphs can be used to find some regularity properties of the entropy $h_\mu(n)$. Concretely, the entropy after n chaotic band reverse bifurcations can be expressed as a function of n and of the entropy in the first chaotic band $h_\mu(0)$. Using the expression of the degree distribution, a little algebra yields:

$$h_\mu(n) = \log 4 + \frac{h_\mu^{\text{top}}(n)}{2^n} = \log 4 + \frac{h_\mu(0)}{2^n}.$$

The chaotic-band reverse bifurcation process in the chaotic region from right to left leads in this case to a decrease of entropy with an asymptotic value of $\log 4$

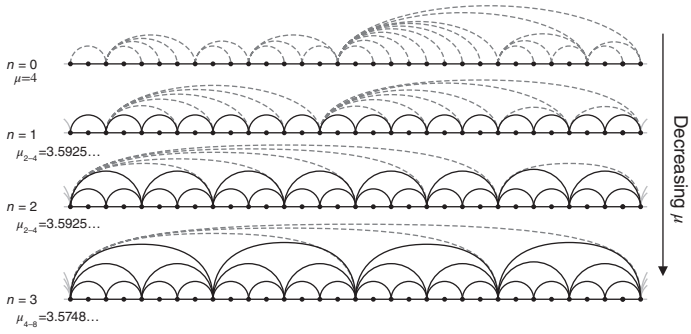

Figure 1.5 Aperiodic Feigenbaum graphs for $\mu > \mu_\infty$. A sequence of graphs associated with chaotic series after n chaotic-band reverse bifurcations, starting at $\mu = 4$ for $n = 0$, when the attractor extends along a single band and the degree distribution does not present any regularity (dashed links). For $n > 0$, the phase space is partitioned in 2^n disconnected chaotic bands and the nth self-affine image of $\mu = 4$ is the nth Misiurewicz point $\mu_{2^{n-1}-2^n}$. In all cases, the orbit visits each chaotic band in the same order as in the periodic region $\mu < \mu_\infty$. This order of visits induces an ordered structure in the graphs (black links) analogous to that found for the period-doubling cascade. (Luque *et al.* [49]. Reproduced with permission of American Institute of Physics.)

for $n \to \infty$ at the accumulation point. These results show that the graph entropy behaves qualitatively as the map's Lyapunov exponent λ, with the peculiarity of having a shift of $\log 4$, as confirmed numerically in Figure 1.6.

This agreement is expected in the chaotic region in view of the Pesin theorem [42], which relates the positive Lyapunov exponents of a map with its Kolmogorov–Sinai entropy (see Eq. 1.9) that for unimodal maps reads $h_{\mathrm{KS}} = \lambda, \forall \lambda > 0$, as we stated that graph entropy h can be used as a proxy for H_{KS}. Unexpectedly, this qualitative agreement seems also valid in the periodic windows ($\lambda < 0$), since the graph entropy is positive and approximately varies with the value of the associated (negative) Lyapunov exponent although $H_{\mathrm{KS}} = 0$, hinting at a Pesin-like relation valid also out of chaos.

In short, graph entropy obtained from the whole structure of the HVg stores much of the information in the dynamic process, and it is a good estimation for the Kolmogorov–Sinai entropy of the original time series. We will see that the same happens with graph block entropies. For this example, we will use another common transition to chaos: intermittency, the seemingly random alternation of long quasi-regular or laminar phases, the so-called intermissions, and relatively short irregular or chaotic bursts. Intermittency is omnipresent in nonlinear science and has been weighed against comparable phenomena in nature, such as Belousov–Zhabotinski chemical reactions, Rayleigh–Benard instabilities, and turbulence [47, 52–54]. Pomeau and Manneville [55] introduced a classification as types I–III for different kinds of intermittency. For definiteness, we chose the case of type I intermittency, as it occurs just preceding an (inverse) tangent bifurcation in nonlinear iterated maps, although the very same methodology can be extended to other situations.

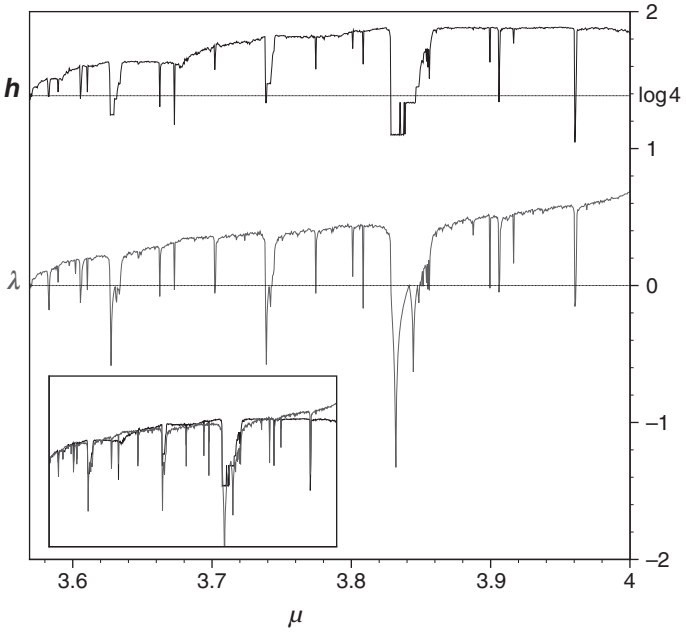

Figure 1.6 Horizontal visibility network entropy h and Lyapunov exponent λ for the Logistic map. We plot the numericalvalues of h and λ for $3.5 < \mu < 4$ (the numerical step is $\delta\mu = 5 \times 10^{-4}$ and in each case the processed time series have a size of 2^{12} data). The inset reproduces the same data but with a rescaled entropy $h - \log(4)$. The surprisingly good match between both quantities is due to the Pesin identity (see text). Unexpectedly, the Lyapunov exponent within the periodic windows ($\lambda < 0$ inside the chaotic region) is also well captured by h. (Luque *et al.* [49]. Reproduced with permission of American Institute of Physics.)

Type I intermittency can be observed infinitely many times in the logistic map

$$x_{t+1} = F(x_t) = \mu x_t(1 - x_t),\ 0 \leq x \leq 1,\ 0 \leq \mu \leq 4, \tag{1.17}$$

close to the control parameter values $\mu = \mu_T$ at which windows of periodicity open with period T for values $\mu > \mu_\infty$. For instance, at $\mu_3 = 1 + \sqrt{8}$, this map exhibits a cycle of period $T = 3$ with subsequent bifurcations. This is the most visible window of periodicity in the chaotic regime (and the one in whose vicinity the following results have been obtained). The regular periodic orbits hold slightly above μ_T, but below μ_T the dynamics consists of laminar episodes interrupted by chaos (i.e., intermittency).

In the bottom part of Figure 1.7, we show the HV graph of the associated intermittent series, which consists of several repetitions of a three-node motif (periodic backbone) linked to the first node of the subsequent laminar trend, interwoven with groups of nodes irregularly (chaotically) connected among them. We observe that the motif repetitions in the graph correspond to the laminar regions in the trajectory (pseudo-periodic data with pseudo-period three) and the chaotically

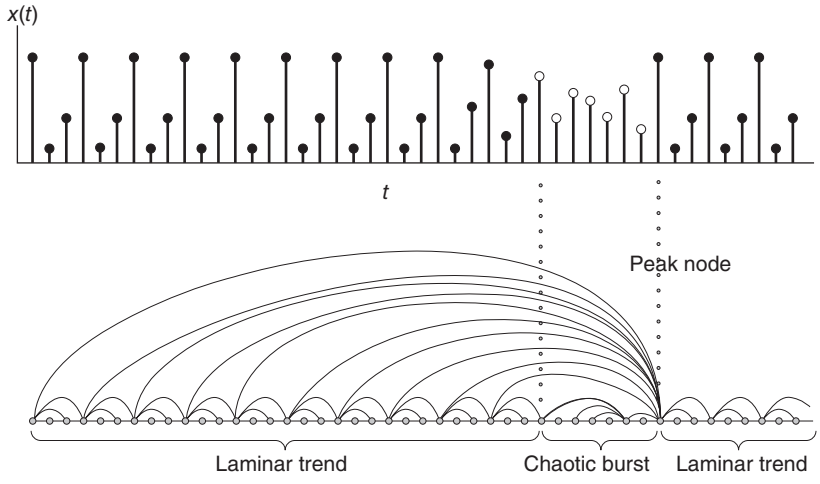

Figure 1.7 Graphical illustration of how the horizontal visibility (HV) graph inherits in its structure the dynamics of the associated intermittent series. In the top of the figure, we show a sample intermittent series generated by the logistic map close to μ_c ($\epsilon > 0$), producing laminar regions (black) mixed with chaotic bursts (white). In the bottom, we plot the associated HV graph. Laminar regions are mapped into nodes with a periodic backbone, whereas the actual pseudo-periodicity of the series is inherited in the graph by the existence of the so-called peak or interfacial nodes. Chaotic bursts are mapped into chaotic nodes, with a characteristic degree distribution. (Núñez *et al.* [56]. Reproduced with permission of American Physical Society.)

connected groups correspond to the chaotic bursts in the trajectory. As laminar trends are indeed pseudo-periodic in the sense that they can be decomposed as a periodic signal and a drift, this pseudo-periodicity expresses in the graph structure by allowing a node for each period-three motif to be connected to the first node in the next laminar region (the so-called peak or interfacial node), as the values of the time series in the chaotic bursts are always smaller than those in the former laminar trend. Therefore, the connectivity of this node is a direct function of the length of the previous laminar phase.

Trajectories generated by canonical models evidencing type I intermittency show power-law scaling in the Lyapunov exponent of the trajectories [55, 57], which reads $\lambda \sim \epsilon^{0.5}$ as $\epsilon \to 0$, where ϵ, called the channel width of the Poincaré section, is the distance between the local Poincaré map and the diagonal [58]. In our case, it is equal to $\epsilon = \mu_T - \mu$. In Figure 1.8, we made a log–log plot of the values of graph block entropies h_n as a function of the channel width ϵ and the block size n. A power law scaling is recovered, albeit with a different scaling exponent $\alpha < 0.5$:

$$h_n \sim \epsilon^{\alpha(n)}. \tag{1.18}$$

As we stated, h_1 (corresponding to the graph entropy, Eq. 1.6) is only a proxy of the Kolmogorov–Sinai entropy of the time series, and thus a comparison with the Lyapunov exponent is only approximate. The same is valid for graph block

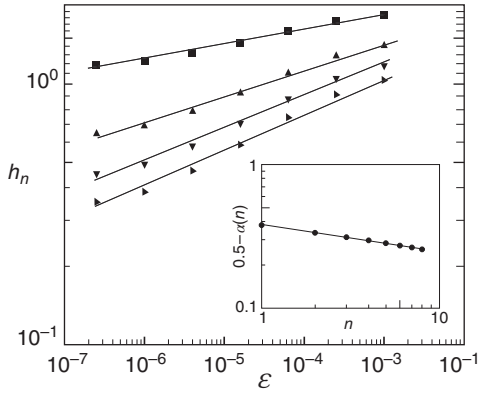

Figure 1.8 Log–log plot of the block entropies h_n constructed from degree distributions of n-sequence of connectivities in the HV graphs as a function of ϵ: $n = 1$ (squares), $n = 2$ (upward-pointing triangles), $n = 3$ (downward-pointing triangles), and $n = 4$ (right triangles). A scaling of the form $h_n \sim \epsilon^{\alpha(n)}$ is found. (Inset panel) Log–log plot of the convergence of $\alpha(n)$ to the exponent associated to the Lyapunov exponent, as a function of n. A relation of the form $[0.5 - \alpha(n)] \sim n^{-0.19}$ is found. (Núñez *et al.* [56]. Reproduced with permission of American Physical Society.)

entropies with $n > 1$, but note that as n increases α decreases according to $[0.5 - \alpha(n)] \sim n^{-0.19}$, converging to 0.5. Here we recall that the limit $n \to \infty$ of graph block entropies h_n was our graph Kolmogorov–Sinai entropy, Eq. 1.12, giving:

$$h_{\mathrm{KS}} = \lim_{n\to\infty} h_n \sim \lim_{n\to\infty} \epsilon^{\alpha(n)} = \epsilon^{0.5} \propto \lambda, \tag{1.19}$$

proving again the relationship between graph entropies and the Pesin theorem. We remark that, whereas the graph entropy and the graph Kolmogorov–Sinai entropy are magnitudes defined in the graph, the Lyapunov exponent is only defined in the system. Still, the strong numerical evidence in favor of a Pesin-like identity between the map's Lyapunov exponent and the entropies defined in the graph support that a graph analogue of the Lyapunov exponent can be defined in the graph space.

1.2.3
Graph Entropy Optimization and Critical Points

The information stored in the graph entropy (Eq. 1.6) allows also to identify the critical points in maps with order-to-chaos transitions. We can arrive to this result via optimization of the entropy. In order to illustrate this, we will consider the logistic map and the period-doubling bifurcation cascade, or Feigenbaum scenario, already considered at the beginning of the previous section. Consider the Lagrangian

$$\mathcal{L} = -\sum_{k=2}^{\infty} p(k)\log p(k) - (\lambda_0 - 1)\left(\sum_{k=2}^{\infty} p(k) - 1\right) - \lambda_1\left(\sum_{k=2}^{\infty} kp(k) - \overline{k}\right),$$

for which the extremum condition reads

$$\frac{\partial \mathcal{L}}{\partial p(k)} = -\log p(k) - \lambda_0 - \lambda_1 k = 0,$$

and has the general solution

$$p(k) = e^{-\lambda_0 - \lambda_1 k}.$$

The Lagrange multipliers λ_0 and λ_1 can be calculated from their associated constraints. First, the normalization of the probability density,

$$\sum_{k=2}^{\infty} e^{-\lambda_0 - \lambda_1 k} = 1,$$

implies the following relation between λ_0 and λ_1

$$e^{\lambda_0} = \sum_{k=2}^{\infty} e^{-\lambda_1 k} = \frac{e^{-\lambda_1}}{e^{\lambda_1} - 1},$$

and differentiation of this last expression with respect to λ_1 yields

$$-\sum_{k=2}^{\infty} k e^{-\lambda_1 k} = \frac{e^{-\lambda_1} - 2}{(e^{\lambda_1} - 1)^2}.$$

Second, the assumption that the mean degree is a well-defined quantity (true for HV graphs) yields

$$\sum_{k=2}^{\infty} k e^{-\lambda_0 - \lambda_1 k} = \overline{k} = \frac{2 - e^{-\lambda_1}}{1 - e^{-\lambda_1}}.$$

Combining the above results, we find

$$\lambda_1 = \log\left(\frac{\overline{k} - 1}{\overline{k} - 2}\right),$$

and

$$\lambda_0 = \log\left(\frac{(\overline{k} - 2)^2}{\overline{k} - 1}\right).$$

Hence, the degree distribution that maximizes h is

$$p(k) = \frac{\overline{k} - 1}{(\overline{k} - 2)^2}\left(\frac{\overline{k} - 2}{\overline{k} - 1}\right)^k,$$

which is an increasing function of $\overline{k}$. The maximal entropy therefore found for the maximal mean degree, which we saw in the section "Natural and Horizontal Visibility algorithms," is $\overline{k} = 4$. This yields an associated degree distribution

$$p(k) = \frac{3}{4}\left(\frac{2}{3}\right)^k = \frac{1}{3}\left(\frac{2}{3}\right)^{k-2},$$

which coincides with the one expected for a random uncorrelated series, as we saw in the aforementioned section. Remarkably, we conclude that the HV graph

with maximal entropy is that associated with a purely uncorrelated random process.

So far, we have not used any property of the Logistic map and their associated Feigenbaum graphs, and hence the previous result is a completely general one. Now we will use them in the form of restrictions to the maximization of the graph entropy. Note that by construction, the Feigenbaum graphs from the Logistic map along the period-doubling route to chaos ($\mu < \mu_\infty$) do not have odd values for the degree. Let us assume now this additional constraint in the former entropy optimization procedure. The derivation proceeds along similar steps, although summations now run only over even terms. Concretely, we have

$$e^{\lambda_0} = \sum_{k=1}^{\infty} e^{-\lambda_1 2k} = \frac{1}{e^{2\lambda_1} - 1},$$

which after differentiation over λ_1 gives

$$\sum_{k=1}^{\infty} k e^{-\lambda_1 2k} = \frac{e^{2\lambda_1} - 2}{(e^{2\lambda_1} - 1)^2}$$

and

$$\sum_{k=1}^{\infty} 2k e^{-\lambda_0 - \lambda_1 2k} = \overline{k} = \frac{2e^{2\lambda_1}}{e^{2\lambda_1} - 1}.$$

We obtain for the Lagrange multipliers

$$\lambda_1 = \frac{1}{2} \log\left(\frac{\overline{k}}{\overline{k} - 2}\right),$$

and

$$\lambda_0 = \log\left(\frac{\overline{k} - 2}{2}\right).$$

The degree distribution that maximizes the graph entropy turns now to be

$$p(k) = \frac{2}{\overline{k} - 2}\left(\frac{\overline{k} - 2}{\overline{k}}\right)^{k/2}.$$

As before, entropy is an increasing function of $\overline{k}$, attaining its larger value for the upper-bound value $\overline{k} = 4$, which reduces to $p(k) = (1/2)^{k/2}$, $k = 2, 4, 6, \ldots$, equation 1.14. We conclude that the maximum entropy of the entire family of Feigenbaum graphs, if we require that odd values for the degree are not allowed, is achieved at the logistic map accumulation point. Finally, the network entropy is trivially minimized for a degree distribution $p(2) = 1$, that is, the HV degree distribution coming from the constant series. In short, the graph entropy optimization leads to three special regimes: random dynamics, constant time series, and the critical accumulation point, where the transition order-to-chaos takes place.

In the case of intermittency also studied in the previous section, it is very evident to show how the graph entropy corresponds to a minimum in the transition point. Eq. 1.18 showed that in this scenario, graph entropy (corresponding to block entropy with $n = 1$) was $h_1 \sim \epsilon^{\alpha(1)}$ (being $\alpha(1) \simeq 0.12$, see inset in Figure 1.8). Clearly, as we approach to the transition point, $\epsilon \to 0$ (i.e., as $\mu \to \mu_c$, coming from the chaotic zone to the ordered period-three window), we obtain $h_1 \to 0$. Hence, graph entropy reaches a global minimum for the HV graph at tangency $\epsilon = 0$ (but note that there is no continuity in h_1: when we effectively arrive to $\epsilon = 0$, suddenly the graph changes radically to an ordered graph with $h_1 = \log 3$).

Finally, we will study a third route to chaos, quasi-periodicity. Quasi-periodicity is observed along time evolution in nonlinear dynamical systems [47, 48, 59] and also in the spatial arrangements of crystals with forbidden symmetries [50, 60]. These two manifestations of quasi-periodicity are rooted in self-similarity and are seen to be related through analogies between incommensurate quantities in time and spatial domains [50]. Quasi-periodicity can be visualized also in the graphs generated when the HV algorithm is applied to the stationary trajectories of the universality class of low-dimensional nonlinear iterated maps with a cubic inflexion point, as represented by the circle map [50].

We briefly recall that the critical circle map [47, 48, 59] is the one-dimensional iterated map given by

$$\theta_{t+1} = f_{\Omega,K}(\theta_t) = \theta_t + \Omega - \frac{1}{2\pi}\sin(2\pi\theta_t), \mathrm{mod}\ 1, \tag{1.20}$$

representative of the general class of nonlinear circle maps: $\theta_{t+1} = f_{\Omega,K}(\theta_t) = \theta_t + \Omega + g(\theta_t), \mathrm{mod}\ 1$, where $g(\theta)$ is a periodic function that fulfills $g(\theta + 1) = g(\theta)$.

The dynamical variable $0 \leq \theta_t < 1$ can be interpreted as a measure of the angle that specifies the trajectory on the unit circle, the control parameter Ω is the so-called *bare winding number*. The *dressed winding number* for the map is defined as the limit of the ratio: $\omega \equiv \lim_{t\to\infty}(\theta_t - \theta_0)/t$ and represents an averaged increment of θ_t per iteration. Trajectories are periodic (locked motion) when the corresponding dressed winding number $\omega(\Omega)$ is a rational number p/q and quasi-periodic when it is irrational. The resulting hierarchy of mode-locking steps at $k = 1$ can be conveniently represented by aFarey tree, which orders all the irreducible rational numbers $p/q \in [0, 1]$ according to their increasing denominators q.

The HV algorithm assigns each datum θ_i of a time series $\{\theta_i\}_{i=1,2,\ldots}$ to a node i in its associated HV graph, and i and j are two connected nodes if $\theta_i, \theta_j > \theta_n$ for all n such that $i < n < j$. The associated HV graph is a periodic repetition of a motif with q nodes, p of which have connectivity $k = 2$. (Observe that p in the map indicates the number of turns in the circle to complete a period). For $k \leq 1$, the order of visits of positions in the attractors and their relative values remain invariant for a locked region with $\omega = p/q$ [61], such that the HV graphs associated with them are the same. In Figure 1.9 we present an example, in which the first and last nodes in the motif correspond to the largest value in the attractor.

In Figure 1.10, we depict the associated HV periodic motifs for each p/q in the Farey tree. We directly observe that the graphs can be constructed by means of

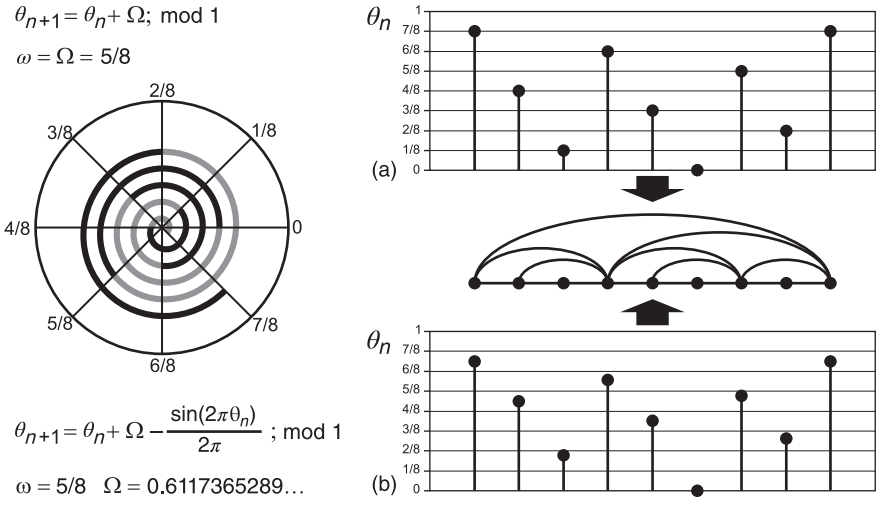

Figure 1.9 Examples of two standard circle map periodic series with dressed winding number $\omega = 5/8$, $K = 0$ (a) and $K = 1$ (b). As can be observed, the order of visits on the circle and the relative values of θ_n remain invariant and the associated HV graph is therefore the same in both cases.

the following inflation process: let p/q be a Farey fraction with "parents" $p'/q' < p''/q''$, that is, $p/q = (p' + p'')/(q' + q'')$. The "offspring" graph $G(p/q)$ associated with $\omega = p/q$, can be constructed by the concatenation $G(p''/q'') \oplus G(p'/q')$ of the graphs of its parents. By means of this recursive construction, we can systematically explore the structure of every graph along a sequence of periodic attractors leading to quasi-periodicity. A standard procedure to study the quasi-periodic route to chaos is selecting an irrational number $\omega_\infty \in [0, 1]$. Then, a sequence ω_n of rational numbers approaching ω_∞ is taken. This sequence can be obtained through successive truncations of the continued fraction expansion of ω_∞. The corresponding bare winding numbers $\Omega(\omega_n)$ provide attractors, whose periods grow toward the onset of chaos, where the period of the attractor must be infinite. A well-studied case is the sequence of rational approximations of $\omega_\infty = \phi^{-1} = (\sqrt{5} - 1)/2 \simeq 0.6180\ldots$, the reciprocal of the Golden ratio, which yields winding numbers $\{\omega_n = F_{n-1}/F_n\}_{n=1,2,3,\ldots}$, where F_n is the Fibonacci number generated by the recurrence $F_n = F_{n-1} + F_{n-2}$ with $F_0 = 1$ and $F_1 = 1$. The first few steps of this route are shown in Figure 1.10(b): $\omega_1 = 1/1, \omega_2 = 1/2, \omega_3 = 2/3, \omega_4 = 3/5, \omega_5 = 5/8\ldots, \omega_6 = 8/13\ldots$. Within the range $\Omega(F_{n-1}/F_n)$, one observes trajectories of period F_n and, therefore, this route to chaos consists of an infinite family of periodic orbits with increasing periods of values F_n, $n \to \infty$. If we denote by $G_{\phi^{-1}}(n)$ the graph associated to $\omega_n = F_{n-1}/F_n$ in the Golden ratio route, it is easy to prove that the associated connectivity distribution $P(k)$ for $G_{\phi^{-1}}(n)$ with $n \geq 3$ and $k \leq n + 1$ is $p_n(2) = F_{n-2}/F_n, p_n(3) = F_{n-3}/F_n, p_n(4) = 0$ and $p_n(k) = F_{n-k+1}/F_n$. In the limit $n \to \infty$ the connectivity distribution at the accumulation point $G_{\phi^{-1}}(\infty)$, the

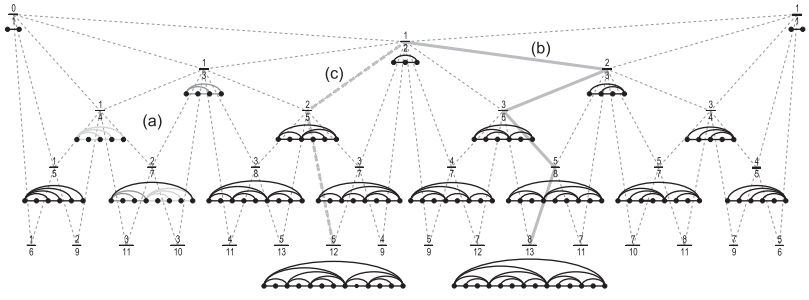

Figure 1.10 Six levels of the Farey tree and the periodic motifs of the graphs associated with the corresponding rational fractions p/q taken as dressed winding numbers ω in the circle map (for space reasons, only two of these are shown at the sixth level). (a) In order to show how graph concatenation works, we have highlighted an example using different gray tones on the left-hand side: as $1/3 > 1/4$, $G(1/3)$ is placed on the left-hand side, $G(1/4)$ on the right-hand side and their extremes are connected to an additional link closing the motif $G(2/7)$. (b) Five steps in the Golden ratio route, $b = 1$ (thick solid line); (c) Three steps in the Silver ratio route, $b = 2$ (thick dashed line).

quasi-periodic graph at the onset of chaos, takes the form

$$p_\infty(k) = \begin{cases} 1 - \phi^{-1} & k = 2 \\ 2\phi^{-1} - 1 & k = 3 \\ 0 & k = 4 \\ \phi^{1-k} & k \geq 5. \end{cases} \tag{1.21}$$

A straightforward generalization of this scheme is obtained by considering the routes $\{\omega_n = F_{n-1}/F_n\}_{n=1,2,3,\ldots}$ with $F_n = bF_{n-1} + F_{n-2}$, $F_0 = 1$, $F_1 = 1$, where b a natural number. It can be easily seen that $\lim_{n\to\infty} F_{n-1}/F_n = (-b + \sqrt{b^2+4})/2$, which is a solution of the equation $x^2 + bx - 1 = 0$. Interestingly, all the positive solutions of the above family of quadratic equations happen to be positive quadratic irrationals in $[0, 1]$ with pure periodic continued fraction representation: $\phi_b^{-1} = [b, b, b, \ldots] = [\overline{b}]$ ($b = 1$ corresponds to the Golden number, $b = 2$ to the Silver number, and so on). Every $b > 1$ fulfills the condition $F_{n-1}/F_n < 1/2$.

For fixed $b \geq 2$, we can deduce from the construction process illustrated in Figure 1.10, and from the balance equation $p_\infty(k) = \phi_b^{-1} p_\infty(k + b)$, that the degree distribution $p_\infty(k)$ for quasi-periodic graphs with $b \geq 2$ is

$$p_\infty(k) = \begin{cases} \phi_b^{-1} & k = 2 \\ 1 - 2\phi_b^{-1} & k = 3 \\ (1 - \phi_b^{-1})\phi_b^{(3-k)/b} & k = bn + 3, n \in \mathbb{N} \\ 0 & \text{otherwise.} \end{cases} \tag{1.22}$$

Let us proceed now with the optimization of graph entropy. It has to take into account the constraints found in the HV graphs from the circle map: $p(2) = \phi_b^{-1}$, $p(3) = 1 - 2\phi_b^{-1}$, mean connectivity $\langle k \rangle = 4$ (as it comes from a non-periodic series), and $p(k) = 0 \quad \forall k \neq bn + 3, n \in \mathbb{N}$. Note that these are in fact the

constraints for $b \geq 2$; for $b = 1$, the first two constraints should be $p(2) = 1 - \phi^{-1}$ and $p(3) = 2\phi^{-1} - 1$ (see Eq. 1.21), but to make this proof as general as possible, we will proceed with $b \geq 2$ and let the case $b = 1$ as an exercise for the reader.

In order to take into account the first two constraints, we define

$$P := 1 - p(2) - p(3) = 1 - \phi_b^{-1} - (1 - 2\phi_b^{-1}) = \phi_b^{-1}, \tag{1.23}$$

that is, the sum of $p(k)$ for $k > 3$. For the third constrain, we define the reduced mean connectivity

$$Q := 4 - 2p(k) - 3p(3) = 1 + 4\phi_b^{-1}; \tag{1.24}$$

therefore, introducing these constraints in the Lagrangian, we have

$$\mathcal{L} = -\sum_{k=3+bn}^{\infty} p(k)\log p(k) - (\lambda_0 - 1)\left(\sum_{k=3+bn}^{\infty} p(k) - P\right) - \lambda_1\left(\sum_{k=3+bn}^{\infty} kp(k) - Q\right),$$

for which the extremum condition reads

$$\frac{\partial \mathcal{L}}{\partial p(k)} = -\log p(k) - \lambda_0 - \lambda_1 k = 0,$$

and has the solution

$$p(k) = e^{-\lambda_0 - \lambda_1 k}.$$

From this, and using the definition of P we get

$$P = \sum_{k>3} p(k) = \sum_{k=3+bn}^{\infty} e^{-\lambda_0 - \lambda_1 k} = e^{-\lambda_0} \sum_{k=3+bn}^{\infty} e^{\lambda_1 k} = \phi_b^{-1}.$$

As the infinite sum gives

$$\sum_{k=3+bn}^{\infty} e^{-\lambda_1 k} = \frac{e^{-(3+b)\lambda_1}}{1 - e^{-b\lambda_1}}, \tag{1.25}$$

we get the following relationship between the Lagrange multipliers:

$$e^{-\lambda_0} = \frac{\phi_b^{-1}(1 - e^{-b\lambda_1})}{e^{-(3+b)\lambda_1}}. \tag{1.26}$$

Using now the reduced mean connectivity Q, we get

$$Q = \sum_{k>3} kp(k) = \sum_{k=3+bn}^{\infty} ke^{-\lambda_0 - \lambda_1 k} = e^{-\lambda_0} \sum_{k=3+bn}^{\infty} ke^{\lambda_1 k} = 1 + 4\phi_b^{-1}. \tag{1.27}$$

In order to calculate the sum, we can derive Eq. 1.25 respect to λ_1, which gives

$$\sum_{k=3+bn}^{\infty} ke^{-\lambda_1 k} = e^{-3\lambda_1}\left\{\frac{3e^{-b\lambda_1}}{1 - e^{-b\lambda_1}} + \frac{be^{-b\lambda_1}(1 - e^{-b\lambda_1}) + be^{-2b\lambda_1}}{(1 - e^{-b\lambda_1})^2}\right\}.$$

Substituting this sum into Eq. 1.27 and using Eq. 1.26, we get

$$1 + 4\phi_b^{-1} = e^{-3\lambda_1}\left\{\frac{3e^{-b\lambda_1}}{1 - e^{-b\lambda_1}} + \frac{be^{-b\lambda_1}(1 - e^{-b\lambda_1}) + be^{-2b\lambda_1}}{(1 - e^{-b\lambda_1})^2}\right\}\frac{\phi_b^{-1}(1 - e^{-b\lambda_1})}{e^{-(3+b)\lambda_1}},$$

which after some algebra, yields

$$\phi_b + 4 = 3 + b + \frac{be^{-b\lambda_1}}{1 - e^{-b\lambda_1}},$$

giving for the second Langrangian multiplier

$$e^{-\lambda_1} = \left(\frac{\phi_b + 1 - b}{\phi_b + 1}\right)^{1/b}.$$

This can be simplified multiplying and dividing by ϕ_b and making use of the relationship for metallic numbers $\phi_b^2 = 1 + b\phi_b$, giving

$$e^{-\lambda_1} = \phi_b^{-\frac{1}{b}}.$$

Introducing it in Eq. 1.26, we get for the first Lagrange multiplier the result

$$e^{-\lambda_0} = \frac{\phi_b^{-1}(1 - e^{-b\lambda_1})}{e^{(3-b)\lambda_1}} = \frac{\phi_b^{-1}(1 - \phi_b^{-1})}{\phi_b^{-\frac{3+b}{b}}} = \phi_b^{\frac{3}{b}}(1 - \phi_b^{-1}).$$

Therefore, the degree distribution maximizing graph entropy in the circle map case is given by

$$p(k) = \begin{cases} \phi_b^{-1} & k = 2 \\ 1 - 2\phi_b^{-1} & k = 3 \\ \phi_b^{\frac{3}{b}}(1 - \phi_b^{-1})\phi_b^{-\frac{k}{b}} & k = bn + 3, n \in \mathbb{N} \\ 0 & \text{otherwise.} \end{cases} \tag{1.28}$$

which is exactly the same as Eq. 1.22. Q.E.D.

1.3 Renormalization Group Transformations of Horizontal Visibility Graphs

The infinite families of graphs generated by the HV algorithm from time series formed by trajectories obtained along the three routes to chaos in low-dimensional maps are particularly suitable objects for exploration via the renormalization group (RG) transformation. The RG method was originally developed in quantum field theory and in statistical mechanics of phase transitions to remove unwanted divergences in relevant quantities by redefining parameters iteratively [62, 63]. The method is capable of handling problems involving many length scales, and was found to be specially tractable and fruitful in nonlinear dynamics, where functional composition appears as the basic operation [47].

The central feature of study of the RG method is that of self-affine structures, and these appear profusely in the prototypical nonlinear one-dimensional iterated maps we chose to use for the assessment of the HV procedure. Some time ago, the transitions from periodic to chaotic motion present in these maps were studied via the RG method with celebrated results [47]. The transformation $\mathcal{T}$ in this case

consists of functional composition and rescaling, such as

$$\mathcal{T}\{f_\mu(x)\} = \alpha f_\mu\left[f_\mu(\alpha^{-1}x)\right], \tag{1.29}$$

where $f_\mu(x)$ is the one-dimensional nonlinear map, for instance, the logistic map, with control parameter μ. Repeated application of $\mathcal{T}$ modifies the original map $f_\mu(x)$ into another map $\mathcal{T}\{f_\mu(x)\}$, a second application into yet another map $\mathcal{T}^{(2)}\{f_\mu(x)\}$, and so on, with $\mathcal{T}^{(n)}\{f_\mu(x)\}$ after n applications. A "flow" is generated in the set of maps that terminates when $n \to \infty$ at a fixed-point map $f^*_\mu(x)$ that satisfies

$$f^*_\mu(x) = \alpha f^*_\mu\left[f^*_\mu(\alpha^{-1}x)\right], \tag{1.30}$$

for a given value of α. The fixed points that occur are classified as trivial or nontrivial according to whether these are reached, respectively, for all nonzero values of a small set of variables called relevant, or only for vanishing values of these variables. In our example, there is only one relevant variable $\Delta\mu \equiv \mu - \mu_c$, where μ_c is the value of the control parameter μ at which a transition from regular to chaotic behavior takes place. The fixed-point maps enjoy a universal quality in the sense that a whole class of maps lead to and share the properties of these maps. This is the case of unimodal (one hump) maps of nonlinearity $z > 1$, where z is the degree of its extremum, so that the logistic map is one member of the universality class of quadratic maps $z = 2$. There is an infinite number of irrelevant variables, those that specify the differences between any given map for a given value of z and its nontrivial fixed-point map $f^*_{\mu_c}(x)$.

An important feature of HV graphs is that each one of them represents a large number of nonlinear map trajectories, that is, many time series lead to the same HV graph, and each of them captures significant characteristics of a class of trajectories. In our case studies, the three routes to chaos, each HV graph represents an attractor. This is illustrated by the HV graphs obtained for the period-doubling cascade shown in Figure 1.4. These sets of graphs are independent of the details of the unimodal map, including the value of z. Therefore, we anticipate that application of RG transformations directly on the HV graphs would lead to a comprehensive description of their self-similar properties and characterization via their fixed-point graphs, in particular those that represent the transitions to chaos.

A guide for the construction of the RG transformation $\mathcal{R}$ appropriate for the HV graphs already described is to observe in them the effect of functional composition of the map under consideration. Thus, we look at the HV graphs obtained for the period-doubling cascade of unimodal maps when $\mu < \mu_\infty$. See the consecutive graphs in Figure 1.4 that are obtained from the original map f_μ via the compositions $f^{(2)}_\mu, f^{(4)}_\mu, \ldots, f^{(2^n)}_\mu, \ldots$ Note that each of these graphs transforms into the previous one if $\mathcal{R}$ is defined as the coarse-graining of every couple of adjacent nodes, where at least one of them has degree $k = 2$ into a block node that inherits the links of the previous two nodes. See Figure 1.11. That is, $\mathcal{R}\{G(1,n)\} = G(1,n-1)$, and therefore an iteration of this process yields an RG flow that converges to the trivial fixed point $\mathcal{R}^{(n)}\{G(1,n)\} = G(1,0) \equiv G_0 = \mathcal{R}\{G_0\}$. This is the stable (trivial) fixed point of the RG flow for all $\mu < \mu_\infty$. We note that there is also only one

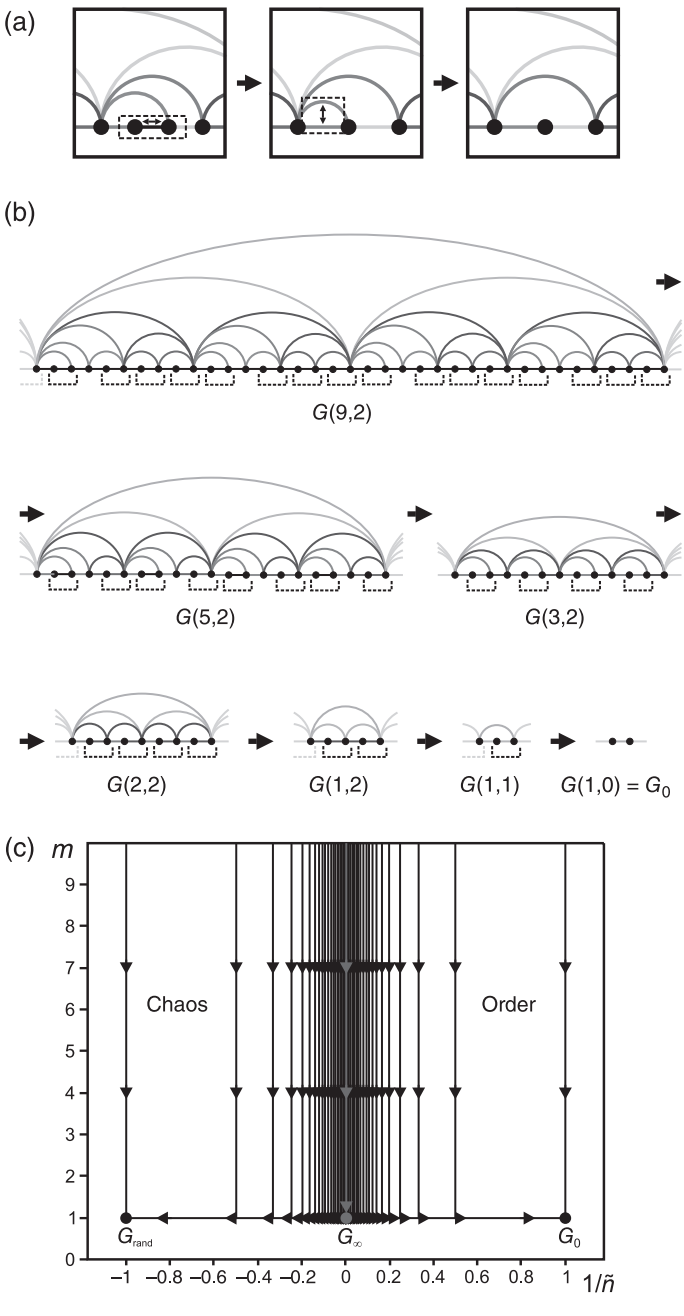

Figure 1.11 Renormalization process and network RG flow structure. (a) Illustration of the renormalization process: a node with degree is coarse-grained with one of its neighbors (indistinctively) into a block node that inherits the links of both nodes. This process coarse-grains every node with the degree of each renormalization step. (b) Example of an iterated renormalization process in a sample Feigenbaum graph at a periodic window with initial period after period-doubling bifurcations (an orbit of period). (c) RG flow diagram.

relevant variable in our RG scheme, represented by the reduced control parameter $\Delta\mu \equiv \mu_c - \mu$, where in this case $\mu_c = \mu_\infty$. Hence, in order to identify a nontrivial fixed point, we set $\Delta\mu = 0$ or equivalently $n \to \infty$, where the structure of the HV graph turns to be completely self-similar under $\mathcal{R}$.

1.3.1 Tangent Bifurcation

A common description of the tangent bifurcation [47] that mediates the transition between a chaotic attractor and an attractor of period T starts with the composition $f^{(T)}$ of a one-dimensional map f, that is, the logistic map, at such bifurcation, followed by an expansion around the neighborhood of one of the T points tangent to the line with unit slope. In general, in the neighborhood of the bifurcation, we have

$$x' = f^{(T)}(x) = x + u\,\mathrm{sign}(x)x^z + \cdots, \;\; z > 1, \tag{1.31}$$

where the most common value for the degree of nonlinearity at tangency is $z = 2$, obtained when the map is analytic at $x = 0$ with nonzero second derivative. When a small constant term $\epsilon \lesssim 0$ is added to Eq. (1.31), we observe in the original map f regular period T orbits, but for $\epsilon \gtrsim 0$, the dynamics associated with f consists of quasi-regular motion while $x_t \simeq 0$, named laminar episodes, interrupted by irregular motion until there is reinjection at a position $x < 0$, that leads to a second laminar episode, and so on, after reinjections at varying positions $x < 0$. The succession of laminar episodes and irregular bursts is known as intermittency of type I [47]. This can be observed at the windows of periodicity of the logistic map that open with period T for values of control parameter $\mu = \mu_T > \mu_\infty$, in which case $\epsilon = \mu_T - \mu$. For convenience, we relabel $\mu_T \equiv \mu_c$. When $\epsilon = 0$ trajectories initiated at $x_0 < 0$ evolve monotonically toward $x = 0$, performing asymptotically a period T orbit in the original map $f(x)$. While trajectories initiated at $x_0 > 0$ move away, also monotonically, from $x = 0$, escaping soon from the local map in Eq. (1.31). In the original map f this leads, after a finite number of iterations, to reinjection at a position $x < 0$ of $f^{(T)}(x)$, followed by repetition of the case $x_0 < 0$.

The RG fixed-point map at the tangent bifurcation, the solution of Eq. (1.30), was obtained in analytical closed-form Ref. [47] together with the specific value $\alpha = 2^{1/(1-z)}$, which upon expansion around $x = 0$ reproduces Eq. (1.31). Here, we are interested in reporting the effect of the transformation $\mathcal{R}$ on the intermittent graphs $G(\epsilon)$ already described. Results for the RG flows include the following [56]:

(i) When $\epsilon < 0$ ($\mu \gtrsim \mu_c$), trajectories are periodic and every HV graph trivially renormalizes toward the chain graph G_0 (an infinite chain with $k = 2$) for all nodes [56]. The graph G_0 is invariant under renormalization $\mathcal{R}\{G_0\} = G_0$, and indeed constitutes a trivial (attractive) fixed point of the RG flow, $\mathcal{R}^{(n)}\{G(\epsilon < 0)\} = G_0$.

(ii) When $\epsilon > 0$ ($\mu \lesssim \mu_c$), repeated RG transformations eliminate progressively the links in the graph associated with correlated elements in the time series,

leading ultimately to the HV graph that corresponds to a random time series G_{rand}. The links between laminar nodes stem mainly from temporal correlated data, whereas the links between burst and peak nodes originate from uncorrelated segments of the time series. If the laminar episodes are eliminated from the time series, the burst and reinjection data values form a new time series, which upon renormalization leads to the random time series. We have $\lim_{n\to\infty} \mathcal{R}^{(n)}\{G(\epsilon > 0)\} = G_{\text{rand}}$, where G_{rand} is the HV graph associated with a random uncorrelated process with the aforementioned graph properties. This constitutes the second trivial (attractive) fixed point of the RG flow [56].

(iii) When $\epsilon = 0$ ($\mu = \mu_c$), the HV graph generated by trajectories at tangency converges after repeated application of $\mathcal{R}$ to a nontrivial fixed point. This occurs after only two steps when $T = 3$, $\mathcal{R}^2\{G(=0)\} = G_c = \mathcal{R}\{G_c\}$ and remains invariant under $\mathcal{R}$ afterward. This feature can be demonstrated by explicit application of $\mathcal{R}$ upon $G(\epsilon = 0)$ (see Figure 1.12 for a graphical illustration of this process). The fixed-point graph G_c is the HV graph of a

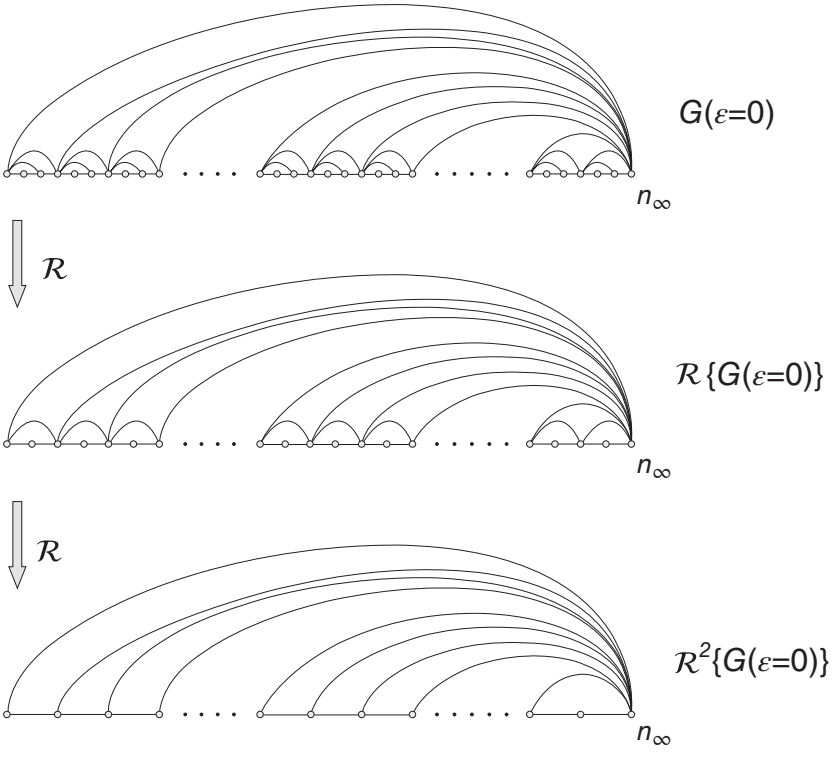

Figure 1.12 Illustration of the renormalization operator $\mathcal{R}$ applied on the HV graph at $\epsilon = 0$. This graph renormalizes, after two iterations of $\mathcal{R}$, into an HV graph G_c which is itself (i) invariant under $\mathcal{R}$ and (ii) unstable under perturbations in ϵ, thus constituting a nontrivial (saddle) fixed point of the graph-theoretical RG flow.

monotonically decreasing time series bounded at infinity by a large value, that of the initial position x_0. The fixed-point graph G_c is unstable under perturbations in ϵ, and it is thus a saddle point of the RG flow, attractive only along the critical manifold [spanned by $G(\epsilon = 0)$ and its replicas within other periodic windows of period T]. The RG flow diagram is shown in Ref. [56].

1.3.2 Period-Doubling Accumulation Point

A classic example of functional composition RG fixed-point map is the solution of Eq. (1.30) associated with the period-doubling accumulation points shared by all unimodal maps [64]

$$f_\mu(x) = 1 - \mu|x|^z, \;\; z > 1, \;\; -1 \le x \le 1, \;\; 0 \le \mu \le 2. \tag{1.32}$$

In practice, it is often numerically illustrated by use of a single map, the quadratic $z = 2$ logistic map with the control parameter located at $\mu = \mu_\infty(1) = 1.401155189092$, the value for the accumulation point of the main period-doubling cascade [47, 64].

Iterating $\mathcal{R}$ on the Feigenbaum graphs, we can trace the RG flows of the period-doubling and band-splitting graphs $G(\Delta\mu)$ already described. A complete schematic representation of the RG flows can be seen in Figure 1.11. Results include the following [21, 49]:

(i) We have seen that when $\Delta\mu(1) < 0$ ($\mu < \mu_\infty(1)$), the RG flow produced by repeated application of $\mathcal{R}$ on the period-doubling cascade of graphs $G(1, n)$ leads to $G_0 \equiv G(1, 0)$, the infinite chain with $k = 2$ for all nodes, that is, $\mathcal{R}\{G_0\} = G_0$ is the trivial (attractive) fixed point of this flow.

(ii) We have also seen that when $\Delta\mu(1) = 0$ ($\mu = \mu_\infty(1)$), the graph $G(1, \infty) \equiv G_\infty$ that represents the accumulation point of the cascade of period 2^∞ is the nontrivial (repulsive) fixed point of the RG flow, $\mathcal{R}\{G_\infty\} \equiv G_\infty$. In connection with this, let $p_t(k)$ be the degree distribution of a generic Feigenbaum graph G_t in the period-doubling cascade after t iterations of $\mathcal{R}$, and point out that the RG operation $\mathcal{R}\{G_t\} \equiv G_{t+1}$ implies a recurrence relation $(1 - p_t(2))p_{t+1}(k) = p_t(k + 2)$, whose fixed point coincides with the degree distribution found for the period-doubling cascade. This confirms that the nontrivial fixed point of the flow is indeed G_∞.

(iii) When $\Delta\mu(1) > 0$ ($\mu > \mu_\infty(1)$) and μ does not fall within a window of periodicity $m > 1$. Under the same RG transformation, the self-affine structure of the family of 2^n-band attractors yields $\mathcal{R}\{G_\mu(1, n)\} = G_\mu(1, n - 1)$, generating an RG flow that converges to the Feigenbaum graph associated to the first chaotic band, $\mathcal{R}^{(n)}\{G_\mu(1, n)\} = G_\mu(1, 0)$. Repeated application of $\mathcal{R}$ breaks temporal correlations in the series, and the RG flow leads to a second trivial fixed point $\mathcal{R}^{(\infty)}\{G_\mu(1, 0)\} = G_{\text{rand}} = \mathcal{R}\{G_{\text{rand}}\}$, where G_{rand} is the HV graph generated by a purely uncorrelated random process. As mentioned above, this graph has a universal degree distribution

$p(k) = (1/3)(2/3)^{k-2}$, independent of the random process underlying probability density.

(iv) When $\Delta\mu(m) < 0$ ($\Delta\mu(m) \equiv \mu_\infty(m) - \mu$), where $\mu_\infty(m)$ is the accumulation point of the period-doubling cascades in the window of periodicity with initial period m. Since the RG transformation specifically applies to nodes with degree $k = 2$, the initial applications of $\mathcal{R}$ only change the core structure of the graph associated with the specific value m (see Figure 1.11 for an illustrative example). The RG flow will therefore converge to the trivial fixed point G_0 via the initial path $\mathcal{R}^{(p)}\{G_\mu(m,n)\} = G_\mu(1,n)$, with $p \leq m$, whereas it converges to the trivial fixed point G_{rand} for $G_\mu(m,n)$ via $\mathcal{R}^{(p)}\{G_\mu(m,n)\} = G_\mu(1,n)$. In the limit of $n \to \infty$, the RG flow proceeds toward the nontrivial fixed point G_∞ via the path $\mathcal{R}^{(p)}\{G(m,\infty)\} = G(1,\infty)$. Incidentally, extending the definition of the reduced control parameter to $\Delta\mu(m) \equiv \mu_\infty(m) - \mu$, the family of accumulation points is found at $\Delta\mu(m) = 0$.

In summary, the repeated application of the RG transformation $\mathcal{R}$ generates flows terminating at two different trivial fixed points G_0 and G_{rand} or at the nontrivial fixed point G_∞. The graph G_0 is a chain graph, in which every node has two links, G_{rand} is a graph associated with a purely random uncorrelated process, whereas G_∞ is a self-similar graph that represents the onset of chaos. The RG properties within the periodic windows are incorporated into a general RG flow diagram. As it is common to all RG applications, crossover phenomenon between these fixed points is present when n is large (or $\mu \simeq \mu_\infty$) for both $\mu < \mu_\infty$ and $\mu > \mu_\infty$. In both cases, the graphs $G(1, n-j)$ and $G_\mu(1, n-j)$ with $j \ll n$ closely resemble the self-similar G_∞ (obtained only when $\mu = \mu_\infty$) for a range of values of the number j of repeated applications of the transformation $\mathcal{R}$ until a clear departure takes place toward G_0 or G_{rand} when j becomes comparable to n. Hence, for instance, the graph $\mathcal{R}^{(j)}\{G_\mu(1,n)\}$will only show its true chaotic nature (and therefore converge to G_{rand}) once j and n are of the same order. In other words, this happens once its degree distribution becomes dominated by the contribution of $p_\mu^{\text{top}}(n,k)$ (alternatively, once the core of the graph, related to the chaotic band structure and the order of visits to chaotic bands, is removed by the iteration of the renormalization process).

1.3.3 Quasi-Periodicity

As with the intermittency and the period-doubling routes, the quasi-periodic route to chaos exhibits universal scaling properties. And an RG approach, analogous to that for the tangent bifurcation and the period-doubling cascade, has been carried out for the critical circle map [47]. The fixed-point map $f^*(\theta)$ of an RG transformation that consists of functional composition and rescaling appropriate for maps with a zero-slope cubic inflection point satisfies

$$f^*(\theta) = \alpha_{\text{gm}} f^* \left(\alpha_{gm} f^*(\alpha_{gm}^{-2}\theta) \right), \tag{1.33}$$

where (for the golden mean route) $\alpha_{\rm gm} = -1.288575$ is a universal constant [47]. We proceed as above and apply the same RG graph transformation $\mathcal{R}$ to the families of HV graphs that represent the quasi-periodic route to chaos associated with the golden mean [65]. Then, we consider other routes associated with other metallic mean numbers. The results are as follows:

(i) We have $\mathcal{R}\{G_{\phi^{-1}}(n)\} = G_{1-\phi^{-1}}(n-1)$ and $\mathcal{R}\{G_{1-\phi^{-1}}(n)\} = G_{\phi^{-1}}(n-1)$, and hence the RG flow alternates between the two mirror routes described previously. If we define the operator "time reverse" by $\overline{G}_{\phi^{-1}}(n) \equiv G_{1-\phi^{-1}}(n)$, the transformation becomes $\overline{\mathcal{R}}\{G_{\phi^{-1}}(n)\} = G_{\phi^{-1}}(n-1)$ and $\overline{\mathcal{R}}\{G_{1-\phi^{-1}}(n)\} = G_{1-\phi^{-1}}(n-1)$. Repeated application of $\mathcal{R}$ yields two RG flows that converge, for n finite, to the trivial fixed point G_0 (a graph with $p(2) = 1$). On the contrary, the quasi-periodic graphs, the accumulation points $n \to \infty$, are nontrivial fixed points of the RG flow: $\overline{\mathcal{R}}\{G_{\phi^{-1}}(\infty)\} = G_{\phi^{-1}}(\infty)$ and $\overline{\mathcal{R}}\{G_{1-\phi^{-1}}(\infty)\} = G_{1-\phi^{-1}}(\infty)$. However, the above RG procedure works only in the case of the golden ratio route. This can be noted by looking at the silver ratio route shown in Figure 1.10. For this reason, the RG transformation was extended to other irrational numbers by constructing an explicit algebraic version of $\mathcal{R}$ and then applying to the Farey fractions associated with the graphs [65]. This is

$$R\left(\frac{p}{q}\right) = \begin{cases} R_1\left(\frac{p}{q}\right) = \frac{p}{q-p} & \text{if } \frac{p}{q} < \frac{1}{2}, \\ R_2\left(\frac{p}{q}\right) = 1 - \frac{q-p}{p} & \text{if } \frac{p}{q} > \frac{1}{2}, \end{cases} \tag{1.34}$$

along with the algebraic analog of the "time reverse" operator $\overline{R}(x) = 1 - R(x)$. Observe that along the golden ratio route, fractions are always greater than $1/2$, and we can therefore renormalize this route by setting

$$\overline{R}\left(\frac{F_{n-1}}{F_n}\right) = \overline{R}_2\left(\frac{F_{n-1}}{F_n}\right) = \frac{F_{n-2}}{F_{n-1}}, \tag{1.35}$$

whose fixed-point equation $\overline{R}(x) = x$ is $x^2 + x - 1 = 0$, with ϕ^{-1} a solution of it. The generalization of this scheme to the metallic number ratios, irrational numbers with simple continued fractions, is obtained by considering the routes $\{3c9_n = F_{n-1}/F_n\}_{n=1,2,3,\ldots}$ with $F_n = bF_{n-1} + F_{n-2}$, $F_0 = 1$, $F_1 = 1$ and b a natural number. It can be easily observed that $\lim_{n\to\infty} F_{n-1}/F_n = (-b + \sqrt{b^2+4})/2$, which is a solution of the equation $x^2 + bx - 1 = 0$. Interestingly, all the positive solutions of the above family of quadratic equations happen to be positive quadratic irrationals in $[0, 1]$ with pure periodic continued fraction representation: $\phi_b^{-1} = [b, b, b, \ldots] = [\overline{b}]$ ($b = 1$ corresponds to the golden route, $b = 2$ to the silver route, etc.). Every $b > 1$ fulfills the condition $F_{n-1}/F_n < 1/2$, and, as a result, we have

$$R\left(\frac{F_{n-1}}{F_n}\right) = R_1\left(\frac{F_{n-1}}{F_n}\right) = \frac{F_{n-1}}{(b-1)F_n + F_{n-2}}. \tag{1.36}$$

The transformation R_1 can only be applied $(b-1)$ times before the result turns greater than $1/2$, so the subsequent application of R followed by reversion yields

$$\overline{R^{(b)}}\left(\frac{F_{n-1}}{F_n}\right) = \overline{R_2}\left[R_1^{(b-1)}\left(\frac{F_{n-1}}{F_n}\right)\right] = \frac{F_{n-2}}{F_{n-1}}. \tag{1.37}$$

It is easy to demonstrate by induction that

$$R_1^{(b-1)}(x) = \frac{x}{1-(b-1)x}, \tag{1.38}$$

whose fixed-point equation $R_1^{(b-1)}(x) = \overline{R_2}[R_1^{(b-1)}(x)] = x$ leads in turn to $x^2 + bx - 1 = 0$, with ϕ_b^{-1} a solution of it. We can proceed in an analogous way for the symmetric case $3c9_n = 1 - (F_{n-1}/F_n)$, but, as the sense of the inequalities for $1/2$ is reversed, the role of the operators R_1 and R_2 must be exchanged. The RG flow results are:

(ii) The graphs for fixed $b \geq 2$ are renormalized via $\overline{R^{(b)}}\{G_{\phi_b^{-1}}(n)\} = G_{\phi_b^{-1}}(n-1)$, and, as before, it is found that iteration of this process yields two RG flows that converge to the trivial fixed point G_0 for n finite. The quasi-periodic graphs, reached as accumulation points ($n \to \infty$), act as nontrivial fixed points of the RG flow, since $\overline{R^{(b)}}\{G_{\phi_b^{-1}}(\infty)\} = G_{\phi_b^{-1}}(\infty)$.

(iii) Again for fixed $b \geq 2$, it is found with the help of the construction process illustrated in Figure 1.10, that $p_\infty(2) = \phi_b^{-1}$, $p_\infty(3) = 1 - 2\phi_b^{-1}$ and $p_\infty(k \neq bn+3) = 0$, $n = 1, 2, 3, \ldots$ Whereas $p_\infty(k = bn+3)$, $n = 1, 2, 3, \ldots$ can be obtained from the condition of RG fixed-point invariance of the distribution, as it implies a balance equation $p_\infty(k) = \phi_b^{-1} p_\infty(k+b)$, whose solution has the form of an exponential tail. The degree distribution $p_\infty(k)$ for these sets of quasi-periodic graphs was given earlier.

1.3.4
Entropy Extrema and RG Transformation

An important question pointed out some time ago [66] is whether there exists a connection between the extremal properties of entropy expressions and the RG approach. Namely, that the fixed points of RG flows can be obtained through a process of entropy optimization, adding to the RG approach a variational quality. The families of HV graphs obtained for the three routes to chaos offer a valuable opportunity to examine this issue. As we have seen, they possess simple closed expressions for the degree distribution $p(k)$ and through them there is, when not analytical, exact quantitative access to their entropy

$$h[p(k)] = -\sum_k p(k) \log p(k). \tag{1.39}$$

On the contrary, these families have been ordered along RG flows and their basic fixed points have been determined. The answer provided by HV graphs to the question posed above is clearly in the affirmative. We give some details below.

1.3.4.1 Intermittency

It is found that the entropy h reaches a minimum value at tangency and that this value is retained for $\epsilon < 0$ [56]. The approach to the minimum, at $h(\epsilon = 0) = \log 3$, for the window of periodicity $T = 3$ of the logistic map can be seen in Figure 1.8. This value is maintained within the window, provided $|\epsilon|$ is below the period-doubling bifurcations that take place there. Hence, entropy reaches a global minimum for the HV graph at tangency. Next, we inquire about the effect of the RG transformations on h. The entropy at the nontrivial fixed point vanishes, as $h[p_{G_c}(k)] \to 0$ when the number of nodes $N \to \infty$, that is, the RG reduces h when $\epsilon = 0$. Also, the RG transformations increase h when $\epsilon > 0$ (as $h[p_{G_{\text{rand}}}(k)] = \log(27/4)$ [21, 49]) and reduce it when $\epsilon < 0$ (since $h[p_{G_0}(k)] = 0$ [21, 49]). When $\epsilon > 0$, the renormalization process of removal at each stage of all nodes with $k = 2$ leads to a limiting renormalized system that consists only of a collection of uncorrelated variables, generating an irreversible flow along which the entropy grows. On the contrary, when $\epsilon < 0$, renormalization increments the fraction of nodes with degree $k = 2$ at each stage driving the graph structure toward the simple chain G_0 and thus decreases its entropy to its minimum value.

1.3.4.2 Period Doubling

As we have seen, the degree distribution $p(k)$ that maximizes h is exactly $p(k) = (1/3)(2/3)^{k-2}$, which corresponds to the distribution for the second trivial fixed point of the RG flow G_{rand}. Alternatively, with the incorporation of the additional constraint that allows only even values for the degree (the topological restriction for Feigenbaum graphs $G(1, n)$), entropy maximization yields a degree distribution that coincides with the one found in the nontrivial fixed point of the RG flow G_∞. Finally, the degree distribution that minimizes h trivially corresponds to G_0, the first trivial fixed point of the RG flow. Remarkably, these results indicate that the fixed-point structure of the RG flow is obtained via optimization of the entropy for the entire family of networks. The network entropy is trivially minimized for a degree distribution $p(2) = 1$, that is, at G_0 with $h = 0$. The entropy h is an increasing function of $\overline{k}$, attaining its larger value for the upper-bound value $\overline{k} = 4$, which reduces to $p(k) = (1/2)^{k/2}$, $k = 2, 4, 6, \ldots$. We conclude that the maximum entropy of the entire family of Feigenbaum graphs (when we require that odd values for the degree are not allowed) is achieved at the accumulation point, that is, at the nontrivial fixed point G_∞ of the RG flow. These results indicate that the fixed-point structure of an RG flow can be obtained from an entropy optimization process, confirming the aforementioned connection.

1.3.4.3 Quasi-periodicity

Notably, all the aforementioned RG flow directions and fixed points for this route to chaos can be derived directly from the information contained in the degree distribution via optimization of the graph entropy functional $h[p(k)]$. The optimization is for a fixed b and takes into account the constraints: $p(2) = \phi_b^{-1}$,

$p(3) = 1 - 2\phi_b^{-1}$, maximum possible mean connectivity $\overline{k} = 4$ and $p(k) = 0$ for all $k \neq bn + 3$, $n = 1, 2, 3, \ldots$. The degree distributions $p(k)$ that maximize $h[p(k)]$ can be proven to be exactly the connectivity distributions in Eqs (1.21) and (1.22) for the quasi-periodic graphs at the accumulation points found above. This establishes a functional relation between the fixed points of the RG flow and the extrema of $h[p(k)]$, as it was verified for the intermittency and the period-doubling routes.

Thus, we observe the familiar picture of the RG treatment of a model phase transition, two trivial fixed points that represent disordered and ordered, or high- and low-temperature phases, and a nontrivial fixed point with scale-invariant properties that represent the critical point. There is only one relevant variable, $\Delta\mu = \mu_c - \mu$, that is necessary to vanish to enable the RG transformation to access the nontrivial fixed point.

1.4 Summary

Visibility algorithm is a tool that allows mapping time series into graphs. This algorithm has been applied with interesting results to several research areas. In this chapter, we have introduced several definitions of entropy applied to visibility graphs: graph entropy, and graph Kolmogorov–Sinai entropy. These entropies defined in the graph are equivalent to Shannon entropy and Kolmogorov–Sinai entropy of the time series.

In fact, we have seen that the former are very good proxies of the latter, and we have found that there is a very good agreement between these entropies and the Lyapunov exponent of the corresponding chaotic time series, in view of the Pesin theorem.

Graph entropy also allows to identify the critical points in chaotic maps, via optimization of this entropy. We have seen that critical points correspond to extremals in the process of graph entropy maximization, which produces degree distribution of the visibility graphs at the critical points and at two trivial points: the random series and constant series.

Finally, we have defined some renormalization processes in the visibility graphs that generate flows leading to the same points than the graph entropy maximization does: two fixed points that represent ordered and disordered phases (i.e., the constant series and the random series, respectively), and a nontrivial fixed point that represents the critical point.

The property that is seldom observed [66] is that an entropy functional, in the present case $h[p(k)]$, varies monotonously along the RG flows and is extremal at the fixed points. A salient feature of the HV studies of the routes to chaos in low-dimensional nonlinear iterated maps, intermittency [56], period doubling [21, 49], and quasi-periodicity [65] is the demonstration that the entropy functional $h[p(k)]$ attains extremal (maxima, minima, or saddle point) values at the RG fixed points.

1.5 Acknowledgments

A. Robledo acknowledges support by DGAPA-UNAM-IN103814 and CONACyT-CB-2011-167978 (Mexican Agencies). F.J. Ballesteros acknowledges support by the project AYA2013-48623-C2-2 and B. Luque by the project FIS2013-41057-P both from the Spanish Ministry of Economy and Competitiveness.

References

1. Lacasa, L., Luque, B., Ballesteros, F., Luque, J., and Nu no, J.C. (2008) From time series to complex networks: the visibility graph. *Proc. Natl. Acad. Sci. U.S.A.*, **105** (13), 4972–4975.
2. Nu nez, A., Lacasa, L., Luque, B., and Gómez, J.P. (2011) *Visibility Algorithms in Graph Theory* (edited by Intech 2011), ISBN: 979-953-307-303-2.
3. Lacasa, L. and Luque, B. (2011) in *Mapping Time Series to Networks: A Brief Overview of Visibility Algorithms in Computer Science Research and Technology*, vol. **3** (ed. J.P. Bauer), Nova Publishers, ISBN: 978-1-61122-074-2.
4. Zhang, J. and Small, M. (2006) Complex network from pseudoperiodic time series: topology versus dynamics. *Phys. Rev. Lett.*, **96** (23), 238701.
5. Xu, X., Zhang, J., and Small, M. (2008) Superfamily phenomena and motifs of networks induced from time series. *Proc. Natl. Acad. Sci. U.S.A.*, **105** (50), 19601–19605.
6. Donner, R.V., Zou, Y., Donges, J.F., Marwan, N., and Kurths, J. (2010) Recurrence networks - a novel paradigm for nonlinear time series analysis. *New J. Phys.*, **12** (3), 033025.
7. Donner, R.V., Small, M., Donges, J.F., Marwan, N., Zou, Y., Xiang, R., and Kurths, J. (2010) Recurrence-based time series analysis by means of complex network methods. *Int. J. Bifurcation Chaos*, **21** (4), 1019–1046.
8. Donner, R.V., Donges, J.F., Zou, Y., and Feldhoff, J.H. (2015) *Complex Network Analysis of Recurrences. Recurrence Quantification*, Springer International Publishing, pp. 101–163.
9. Campanharo, A.S.L.O., Sirer, M.I., Malmgren, R.D., Ramos, F.M., and Amaral, L.A.N. (2011) Duality between time series and networks. *PLoS ONE*, **6** (8), e23378.
10. Shirazi, A.H., Jafari, G.R., Davoudi, J., Peinke, J., Tabar, M.R.R., and Sahimi, M. (2011) Mapping stochastic processes onto complex networks. *J. Stat. Mech. Theory Exp.*, **2009** (07), P07046.
11. Strozzi, F., Zaldívar, J.M., Poljansek, K., Bono, F., and Gutiérrez, E. (2009) From Complex Networks to Time Series Analysis and Viceversa: Application to Metabolic Networks. JRC Scientific and Technical Reports, EUR 23947, JRC52892.
12. Haraguchi, Y., Shimada, Y., Ikeguchi, T., and Aihara, K. (2009) Transformation from complex networks to time series using classical multidimensional scaling. *Proceedings of the 19th International Conference on Artificial Neural Networks, ICANN 2009*, Springer-Verlag, Heidelberg, Berlin.
13. Shimada, Y., Ikeguchi, T., and Shigehara, T. (2012) From networks to time series. *Phys. Rev. Lett.*, **109** (15), 158701.
14. Watts, D.J. and Strogatz, S.H. (1998) Collective dynamics of 'small-world' networks. *Nature*, **393**, 440–442.
15. Gao, Z. and Jin, N. (2009) Complex network from time series based on phase space reconstruction. *Chaos*, **19** (3), 033137.
16. Sinatra, R., Condorelli, D., and Latora, V. (2010) Networks of motifs from sequences of symbols. *Phys. Rev. Lett.*, **105** (17), 178702.

17. Sun, X., Small, M., Zhao, Y., and Xue, X. (2014) Characterizing system dynamics with a weighted and directed network constructed from time series data. *Chaos*, **24**, 024402, doi: 10.1063/1.4868261.
18. Luque, B., Lacasa, L., Balleteros, F., and Luque, J. (2009) Horizontal visibility graphs: exact results for random time series. *Phys. Rev. E*, **80** (4), 046103.
19. Gutin, G., Mansour, T., and Severini, S. (2011) A characterization of horizontal visibility graphs and combinatorics on words. *Physica A*, **390** (12), 2421–2428.
20. Lacasa, L. and Toral, R. (2010) Description of stochastic and chaotic series using visibility graphs. *Phys. Rev. E*, **82** (3), 036120.
21. Luque, B., Lacasa, L., Ballesteros, F.J., and Robledo, A. (2011) Feigenbaum graphs: a complex network perspective of chaos. *PLoS ONE*, **6** (9), e22411.
22. Nú nez, A.M., Lacasa, L., Valero, E., Gómez, J.P., and Luque, B. (2012) Detecting series periodicity with horizontal visibility graphs. *Int. J. Bifurcation Chaos*, **22** (7), 1250160.
23. Aguilar-San Juan, B. and Guzman-Vargas, L. (2013) Earthquake magnitude time series: scaling behavior of visibility networks. *Eur. Phys. J. B*, **86**, 454.
24. Telesca, L. and Lovallo, M. (2012) Analysis of seismic sequences by using the method of visibility graph. *Eur. Phys. Lett.*, **97** (5), 50002.
25. Telesca, L., Lovallo, M., and Laszlo, T. (2014) Visibility graph analysis of 2002–2011 Pannonian seismicity. *Physica A*, **416**, 219–224.
26. Telesca, L., Lovallo, M., Ramirez-Rojas, A., and Flores-Marquez, L. (2014) Relationship between the frequency magnitude distribution and the visibility graph in the synthetic seismicity generated by a simple stick-slip system with asperities. *PLoS ONE*, **9** (8), e106233, doi: 10.1371/journal.pone.0106233.
27. Elsner, J.B., Jagger, T.H., and Fogarty, E.A. (2009) Visibility network of United States hurricanes. *Geophys. Res. Lett.*, **36** (16), L16702.
28. Liu, C., Zhou, W.-X., and Yuan, W.-K. (2010) Statistical properties of visibility graph of energy dissipation rates in three-dimensional fully developed turbulence. *Physica A*, **389** (13), 2675–2681.
29. Yang, Y., Jianbo, W., Yang, H., and Mang, J. (2009) Visibility graph approach to exchange rate series. *Physica A*, **388** (20), 4431–4437.
30. Qian, M.-C., Jiang, Z.-Q., and Zhou, W.-X. (2010) Universal and nonuniversal allometric scaling behaviors in the visibility graphs of world stock market indices. *J. Phys. A: Math. Theor.*, **43** (33), 335002.
31. Shao, Z.-G. (2010) Network analysis of human heartbeat dynamics. *Appl. Phys. Lett.*, **96** (7), 073703.
32. Dong, Z. and Liâ, X. (2010) Comment on Network analysis of human heartbeat dynamics. *Appl. Phys. Lett.*, **96** (26), 266101.
33. Ahmadlou, M., Adeli, H., and Adeli, A. (2010) New diagnostic EEG markers of the Alzheimer's disease using visibility graph. *J. Neural Transm.*, **117** (9), 1099–1109.
34. Rashevsky, N. (1955) Life information theory and topology. *Bull. Math. Biophys.*, **17** (3), 229–235.
35. Trucco, E. (1956) A note on the information content of graphs. *Bull. Math. Biol.*, **18** (2), 129–135.
36. Mowshowitz, A. (1968) Entropy and the complexity of graphs (I to IV). *Bull. Math. Biophys.*, **30** (3), 387–414.
37. Körner, J. (1973) Coding of an information source having ambiguous alphabet and the entropy of graphs. Transactions of the 6th Prague Conference on Information Theory, 1971, Academia, Prague, pp. 411–425.
38. Dehmer, M. and Mowshowitz, A. (2011) A history of graph entropy measures. *Inf. Sci.*, **181** (1), 57–78.
39. Shannon, D.E. (1948) A mathematical theory of communication. *Bell Syst. Tech. J.*, **27** (3), 379–423.
40. Kolmogorov, A.N. (1965) Three approaches to the quantitative definition of information. *Probab. Inf. Transm.*, **1** (1), 1–7.
41. Sinai, Ya.G. (1959) On the concept of entropy for dynamical systems. *Dokl.*

Acad. Nauk, **SSSR124**, 768–771 (in Russian).

42. Pesin, Y. (1997) *Dimension Theory in Dynamical Systems: Contemporary Views and Applications*, University of Chicago Press, Chicago.
43. Lagues, M. and Lesne, A. (2011) *Invariances d'echelle*, 2nd edn, Berlin, Paris. English traduction Scaling, Springer Berlin.
44. Castiglione, P., Falcioni, M., Lesne, A., and Vulpiani, A. (2008) *Chaos and Coarse-Graining in Statistical Mechanics*, Cambridge University Press, Cambridge.
45. Karamanos, K. and Nicolis, G. (1999) Symbolic dynamics and entropy analysis of Feigenbaum limit sets. *Chaos, Solitons Fractals*, **10** (7), 1135–1150.
46. Peitgen, H.O., Jurgens, H., and Saupe, D. (1992) *Chaos and Fractals: New Frontiers of Science*, Springer-Verlag, New York.
47. Schuster, H.G. (1988) *Deterministic Chaos. An Introduction*, 2nd revised edn, VCH Publishers, Weinheim.
48. Strogatz, S.H. (1994) *Nonlinear Dynamics and Chaos*, Perseus Books Publishing, LLC.
49. Luque, B., Lacasa, L., Ballesteros, F.J., and Robledo, A. (2012) Analytical properties of horizontal visibility graphs in the Feigenbaum scenario. *Chaos*, **22** (1), 013109.
50. Schroeder, M. (1991) *Fractals, Chaos, Power Laws: Minutes from An Infinite Paradise*, Freeman and Co., New York.
51. Crutchfield, J.P., Farmer, J.D., and Huberman, B.A. (1982) Fluctuations and simple chaotic dynamics. *Phys. Rep.*, **92** (2), 45–82.
52. Maurer, J. and Libchaber, A. (1980) Effect of the Prandtl number on the onset of turbulence in liquid 4He. *J. Phys. Lett.*, **41** (21), 515–518.
53. Pomeau, Y., Roux, J.C., Rossi, A., Bachelart, S., and Vidal, C. (1981) Intermittent behaviour in the Belousov-Zhabotinsky reaction. *J. Phys. Lett.*, **42** (13), 271–273.
54. Bergé, P., Dubois, M., Manneville, P., and Pomeau, Y. (1980) Intermittency in Rayleigh-Bénard convection. *J. Phys. Lett.*, **41** (15), 341–345.
55. Manneville, P. and Pomeau, Y. (1980) Intermittent transition to turbulence in dissipative dynamical systems. *Commun. Math. Phys.*, **74** (2), 189–197.
56. Nú nez, A., Luque, B., Lacasa, L., ómez, J.P.G., and Robledo, A. (2013) Horizontal visibility graphs generated by type-I intermittency. *Phys. Rev. E*, **87** (5), 052801.
57. Hirsch, J.E., Huberman, B.A., and Scalapino, D.J. (1982) Theory of intermittency. *Phys. Rev. A*, **25** (1), 519–532.
58. Kim, M.C., Kwon, O.J., Lee, E.K., and Lee, H. (1994) New characteristic relations in type-I intermittency. *Phys. Rev. Lett.*, **73** (4), 525–528.
59. Hilborn, R.C. (1994) *Chaos and Nonlinear Dynamics*, Perseus Books Publishing, LLC.
60. Shechtman, D., Blech, I., Gratias, D., and Cahn, J.W. (1984) Metallic phase with long-range orientational order and no translational symmetry. *Phys. Rev. Lett.*, **53** (20), 1951–1953.
61. Hao, B.-H. and Zeng, W.-M. (1998) *Applied Symbolic Dynamics and Chaos*, World Scientific Publishing Co., Singapore.
62. Zinn-Justin, J. (2002) *Quantum Field Theory and Critical Phenomena*, Clarendon Press, Oxford, ISBN: 0-19-850923-5.
63. Maris, H.J. and Kadanoff, L.P. (1978) Teaching the renormalization group. *Am. J. Phys.*, **46** (6), 652–657.
64. van der Weele, J.P., Capel, H.W., and Kluiving, R. (1987) Period doubling in maps with a maximum of order z. *Physica A*, **145** (3), 425–460.
65. Luque, B., Nú nez, A., Ballesteros, F., and Robledo, A. (2013) Quasiperiodic graphs: structural design, scaling and entropic properties. *J. Nonlinear Sci.*, **23** (2), 335–342.
66. Robledo, A. (1999) Renormalization group, entropy optimization, and nonextensivity at criticality. *Phys. Rev. Lett.*, **83** (12), 2289–2292.